

1 **Title:** The Jumonji-C oxygenase JMJD7 catalyzes (3*S*)-lysyl hydroxylation of TRAFAC GTPases

2

3 **Author List**

4 Suzana Markolovic<sup>1,7</sup>, Qinqin Zhuang<sup>2,7</sup>, Sarah E Wilkins<sup>1,8</sup>, Charlotte D Eaton<sup>2,8</sup>, Martine I  
5 Abboud<sup>1,8</sup>, Maximiliano J Katz<sup>3,8</sup>, Helen E McNeil<sup>2</sup>, Robert K Leśniak<sup>1</sup>, Charlotte Hall<sup>2</sup>, Weston B  
6 Struwe<sup>1</sup>, Rebecca Konietzny<sup>4</sup>, Simon Davis<sup>4</sup>, Ming Yang<sup>4,5</sup>, Wei Ge<sup>1</sup>, Justin LP Benesch<sup>1</sup>, Benedikt M  
7 Kessler<sup>4</sup>, Peter J Ratcliffe<sup>4,5</sup>, Matthew E Cockman<sup>4,5</sup>, Roman Fischer<sup>4</sup>, Pablo Wappner<sup>3</sup>,  
8 Rasheduzzaman Chowdhury<sup>1,6\*</sup>, Mathew L Coleman<sup>2,9\*</sup>, and Christopher J Schofield<sup>1,9\*</sup>

9

10 **Author Affiliations**

11 <sup>1</sup>Chemistry Research Laboratory, Department of Chemistry, University of Oxford, Oxford, United  
12 Kingdom.

13 <sup>2</sup>Institute of Cancer and Genomic Sciences, University of Birmingham, Birmingham, United  
14 Kingdom.

15 <sup>3</sup>Instituto Leloir, Buenos Aires, Argentina.

16 <sup>4</sup>Target Discovery Institute, University of Oxford, Oxford, United Kingdom.

17 <sup>5</sup>The Francis Crick Institute, London, United Kingdom.

18 <sup>6</sup>Present address: Stanford University School of Medicine, Department of Molecular and Cellular  
19 Physiology, Clark Center, Stanford, CA, USA.

20

21 <sup>7,8,9</sup>These authors contributed equally to this work.

22 \*To whom correspondence should be addressed. E-mail: rasheduzzaman.chowdhury@stanford.edu,  
23 m.coleman@bham.ac.uk, christopher.schofield@chem.ox.ac.uk.

## 24 **ABSTRACT**

25 Biochemical, structural, and cellular studies reveal Jumonji-C (JmjC) domain-containing 7 (JMJD7)  
26 as a 2-oxoglutarate (2OG)-dependent oxygenase catalyzing a previously unreported type of post-  
27 translational modification, (3*S*)-lysyl hydroxylation. Crystallographic analyses reveal JMJD7 as more  
28 closely related to the JmjC hydroxylases rather than the JmjC demethylases. Biophysical and mutation  
29 studies show that JMJD7 has a unique dimerization mode, with interactions between monomers  
30 involving both *N*- and *C*-terminal regions and disulfide bond formation. A proteomic approach  
31 identifies two related members of the Translation Factor (TRAFAC) family of GTPases,  
32 Developmentally Regulated GTP Binding Proteins 1 and 2 (DRG1/2), as activity-dependent JMJD7  
33 interactors. Mass spectrometric analyses demonstrate that JMJD7 catalyzes Fe(II)- and 2OG-  
34 dependent hydroxylation of a highly-conserved lysine residue in DRG1/2; amino acid analyses reveal  
35 JMJD7 catalyzes (3*S*)-lysyl hydroxylation. The functional assignment of JMJD7 will enable future  
36 studies to define the role of DRG hydroxylation in cell growth and disease.

37

## 38 **INTRODUCTION**

39 Following their initial identification as pro-collagen prolyl and lysyl hydroxylases, Fe(II) and 2-  
40 oxoglutarate (2OG)-dependent oxygenases have emerged as widespread regulators of protein  
41 biosynthesis<sup>1,2</sup>. The hypoxia inducible factor prolyl- and asparaginyl- hydroxylases regulate the levels  
42 and transcriptional activity of the  $\alpha\beta$ -hypoxia inducible transcription factors (HIFs). Prolyl  
43 hydroxylation, by the prolyl hydroxylase domain (PHDs/EGLNs) oxygenases, regulates HIF- $\alpha$   
44 subunit levels by signaling for degradation, while asparaginyl hydroxylation (catalyzed by Factor  
45 inhibiting hypoxia inducible factor, FIH) regulates HIF transcriptional activity; the sensitivity of the  
46 PHDs and FIH catalysis to cellular oxygen availability enable them to act as hypoxia sensors<sup>3</sup>. FIH,  
47 but not the PHDs, is a member of the Jumonji-C (JmjC) subfamily of 2OG oxygenases<sup>4</sup>, other  
48 members of which regulate transcription via demethylation of the three histone lysine N<sup>c</sup>-methylation  
49 states. JmjC histone demethylase (KDM) catalysis proceeds via hydroxylation to give a hemiaminal  
50 intermediate, which fragments to give the demethylated product and formaldehyde<sup>5</sup>. There are ~6  
51 human JmjC KDM subfamilies, which are being studied due to their roles in transcription and links to

52 cancer and genetic disorders resulting from mutations to them<sup>6</sup>. 2OG oxygenases are current  
53 therapeutic targets with compounds being developed for clinical applications in cancer (e.g. KDM5  
54 inhibitors)<sup>7</sup> and anemia (PHD inhibitors)<sup>8</sup>.

55  
56 With the exception of FIH, there are limited reports on the ~10 human JmjC oxygenases that catalyze  
57 formation of stable alcohol products ('JmjC hydroxylases'), which are less well-studied than the JmjC  
58 KDMs. In addition to HIF- $\alpha$  isoforms, FIH catalyzes modification of ankyrin repeat domains<sup>9</sup>, and  
59 Jumonji domain-containing 6 (JMJD6) catalyzes hydroxylation of splicing regulatory proteins<sup>10</sup>. JmjC  
60 hydroxylases also have ancient roles in regulation of protein biosynthesis by modifying the  
61 translational machinery<sup>11</sup>. The ribosomal oxygenases (RiOX), MYC-induced nuclear antigen  
62 (MINA53) and nucleolar protein 66 (NO66) catalyze histidinyl hydroxylation of Rpl27a and Rpl8,  
63 respectively<sup>12</sup>. tRNA yW-synthesizing enzyme 5 (TYW5) is a tRNA hydroxylase<sup>13</sup>, and Jumonji  
64 domain-containing 4 (JMJD4) catalyzes hydroxylation of eukaryotic release factor 1 (eRF1), a  
65 reaction increasing stop codon recognition efficiency<sup>14</sup>. In eukaryotes ranging from yeasts to humans,  
66 a 2OG oxygenase that is not a JmjC protein (human: OGFOD1; *Drosophila*: Sudestada1), but which  
67 is related to the HIF PHDs, catalyzes hydroxylation of a prolyl residue in close contact with mRNA in  
68 ribosomes<sup>15</sup>. Overall, these results indicate that multiple 2OG oxygenases are involved in regulation  
69 of protein synthesis at both transcriptional and translational levels<sup>2,15</sup>.

70  
71 Jumonji domain-containing 7 (JMJD7) is one of the few remaining biochemically uncharacterized  
72 human JmjC oxygenases; structure-based bioinformatics predicts it is an Fe(II) and 2OG-dependent  
73 oxygenase containing a JmjC catalytic domain (**Supplementary Fig. 1**). We report biochemical,  
74 crystallographic, and cellular studies revealing JMJD7 as a structurally distinct JmjC hydroxylase  
75 catalyzing a previously unreported post-translational modification (PTM), (3S)-lysyl hydroxylation, in  
76 two related members of the Translation Factor (TRAFAC) GTPase family. The results will enable  
77 future work to elucidate the biological roles of JMJD7 in protein synthesis, the regulation of cell  
78 growth, and disease.

79

80

## 81 RESULTS

### 82 *JMJD7 suppresses cell growth in Drosophila*

83 In an RNAi-based screen for variations in size of the *Drosophila* posterior wing compartment, we  
84 observed that knockdown of CG10133 mRNA, the *Drosophila* orthologue of human JMJD7  
85 (dmJMJD7, 45% sequence identity), correlates with increased posterior wing compartment size, likely  
86 through an increase in cell size (**Supplementary Fig. 2**). Among human JmjC proteins, structure-  
87 based bioinformatics predicts JMJD7 is most closely related to FIH<sup>4</sup>, TYW5<sup>13</sup>, Jumonji domain-  
88 containing 5 (JMJD5)<sup>16</sup>, and the RiOXs, MINA53 and NO66<sup>11</sup>, all of which are JmjC hydroxylases  
89 with roles in protein biosynthesis regulation (in some cases, they are also reported to have KDM  
90 activities). Because the catalytic activities and structures of the JmjC oxygenases can relate to their  
91 physiological roles<sup>17</sup>, we undertook biochemical studies on JMJD7.

92

### 93 *JMJD7 is structurally similar to JmjC hydroxylases*

94 Analysis of the activity of recombinant JMJD7 using <sup>1</sup>H NMR reveals slow Fe(II)-stimulated  
95 conversion of 2OG to succinate in the absence of a substrate (**Supplementary Fig. 3**). As observed  
96 for some other 2OG oxygenases, this conversion was reduced by the broad spectrum inhibitor, *N*-  
97 oxalylglycine (NOG)<sup>18</sup>; alanine substitution of one of the predicted Fe(II)-binding residues (H178)  
98 also reduces 2OG turnover (**Supplementary Figs. 1 and 3b-c**). To support biochemical  
99 characterization of JMJD7 and to investigate whether it functions as a hydroxylase and/or KDM, we  
100 then worked to solve crystal structures for human JMJD7.

101

102 A structure of full-length His<sub>6</sub>-tagged JMJD7 complexed with 2OG and Mn(II), an inert Fe(II)  
103 substitute, was solved by molecular replacement (**Fig. 1**). We obtained a higher resolution (2.2 Å)  
104 structure of a JMJD7 variant arising from a missense mutation (R260C) present in endometrial  
105 cancer<sup>19</sup> and autism<sup>20</sup> (**Supplementary Fig. 1**), the fold of which is very similar to wildtype (0.35 Å  
106 C $\alpha$  root mean squared deviation; **Supplementary Fig. 4 and Supplementary Table 1**). JMJD7  
107 crystallizes as an oligomer with two or four molecules in each asymmetric unit (**Fig. 1 and**  
108 **Supplementary Fig. 4**). Biophysical analyses reveal JMJD7 as dimeric in solution, consistent with

109 immunoprecipitation studies in cells (**Supplementary Fig. 5a-c**). Uniquely among characterized  
110 JmjC proteins, JMJD7 dimerization involves hydrophobic interactions between  $\alpha$ -helices from *both*  
111 *N*- and *C*-terminal regions ( $\alpha 1$ ,  $\alpha 2$ , and  $\alpha 9$ , respectively) and a disulfide involving Cys-47 from two  
112 monomers (**Fig. 1a**; **Supplementary Figs 5d-e** and **6**). The dimeric state of JMJD7 suggests a closer  
113 structural similarity to the JmjC hydroxylases, rather than the demethylases<sup>17</sup>, since the former are  
114 commonly observed as dimers: FIH<sup>21</sup> and TYW5<sup>13</sup> oligomerize via *C*-terminal  $\alpha$ -helical bundles,  
115 while MINA53 and NO66 oligomerize via  $\alpha$ -helical bundles located between their JmjC and winged-  
116 helix domains<sup>11</sup> (**Supplementary Fig. 5e**).

117  
118 The structures reveal each JMJD7 molecule is comprised of 9  $\alpha$ -helices, 18  $\beta$ -strands, and 2-3<sub>10</sub>  
119 helices. The catalytic domain contains the characteristic 2OG oxygenase distorted double-stranded  $\beta$ -  
120 helix (DSBH) core barrel, formed from 8  $\beta$ -strands, arranged as 2 antiparallel major ( $\beta I$ ,  $\beta VIII$ ,  $\beta III$ ,  
121  $\beta VI$ ) and minor ( $\beta II$ ,  $\beta VII$ ,  $\beta IV$ ,  $\beta V$ ) sheets<sup>17</sup>. The DSBH houses the active site, where the 2OG oxalyl  
122 group, water, and the metal-binding triad (H178, D180, and H277) coordinate the metal in an  
123 octahedral geometry (**Fig. 1b**). The 2OG C1 carboxylate is positioned to make a hydrogen bonding  
124 network with the amides of N184 and N289. As with most structurally characterized JmjC  
125 oxygenases, the 2OG C5 carboxylate interacts via electrostatic and hydrogen bonding interactions  
126 with a lysine (K193) on  $\beta IV$ <sup>17</sup>. Most 2OG oxygenases have 2 or 3 polar side-chains positioned to  
127 interact with the 2OG C5 carboxylate group; notably, JMJD7 has 4 such side-chains. In addition to  
128 K193, the hydroxyls of Y127, T175, and Y186 form additional hydrogen bonds with the 2OG C5  
129 carboxylate group (**Fig. 1b**). The apparently tight binding of 2OG is consistent with the observed slow  
130 substrate uncoupled 2OG turnover (**Supplementary Fig. 3**).

131  
132 Comparison of the JMJD7 active site with those of other JmjC oxygenases reveals closer structural  
133 similarity with JmjC hydroxylases than KDMs. Notably, binding of the 2OG C1 carboxylate,  
134 involving hydrogen bonds with the N184 and N289 side-chain amides, emulates interactions made by  
135 FIH<sup>4</sup>, i.e. with the N205<sub>FIH</sub> and N294<sub>FIH</sub> side-chains (**Supplementary Fig. 7a**). Importantly, JMJD7

136 lacks a hydrophobic region crucial in binding the N<sup>ε</sup>-methyl lysine group of the JmjC KDMs<sup>17</sup>. Most  
137 JmjC KDMs tend to have an extended loop at the N-terminus of DSBH βI that is involved in substrate  
138 binding; this is shortened in JMJD7 as in other JmjC hydroxylases (**Supplementary Fig. 7b**)<sup>17</sup>.  
139 Consistent with the absence of structural domains associated with KDM activity (e.g. characteristic  
140 histone- and nucleic acid-binding domains; **Supplementary Fig. 7c**), a panel of histone H3.1  
141 fragments known to be JmjC KDM substrates were not modified by JMJD7 (**Supplementary Fig. 8**).  
142 Overall, the combined biophysical analyses reveal JMJD7 as having greater structural similarity to the  
143 JmjC hydroxylases than the JmjC KDMs.

144

#### 145 *Proteomics identifies TRAFAC GTPases as JMJD7 interactors*

146 To identify potential JMJD7 substrates, we used mass spectrometry (MS) to compare the proteins  
147 interacting with wildtype and (near) inactive (H178A) JMJD7, using dimethyl-N-oxalylglycine  
148 (DMOG), a cell-penetrating precursor of NOG<sup>14</sup>, to trap substrates. Immunoaffinity purifications from  
149 extracts of DMOG-treated cells expressing FLAG-tagged wildtype or JMJD7 H178A were analyzed.  
150 JMJD7-specific interactions ablated by the H178A mutation included two closely related GTPases,  
151 Developmentally Regulated GTP Binding Proteins 1 and 2 (DRG1/2), and their respective binding  
152 partners, DRG family regulatory proteins 1 and 2 (DFRP1/2) (**Fig. 2a** and **Supplementary Fig. 9a**)<sup>22</sup>.  
153 Known JmjC hydroxylase substrates (e.g. eRF1, splicing factors, HIFα, Rpl27a/Rpl8), ankyrins, or  
154 KDM substrates (e.g. histones) were not detected. Activity-dependent interactions of JMJD7 with  
155 DRG1 and DRG2 were confirmed in different cell lines (**Supplementary Fig. 9b-d**). Reciprocal  
156 immunoprecipitations using FLAG-tagged DRGs confirmed the interaction with endogenous JMJD7,  
157 but not the related hydroxylase JMJD4 (**Supplementary Fig. 9e**). Importantly, purification of  
158 endogenous DRG/DFRP complexes also co-precipitated endogenous JMJD7 (but not JMJD4; **Fig.**  
159 **2b**). To investigate whether JMJD7 and DRG1/2 co-localize, immunofluorescence staining of co-  
160 expressed JMJD7 and DRG1 or DRG2 was performed in HeLa cells (**Fig. 2c**). Consistent with the  
161 proteomic and co-immunoprecipitation data, we observed significant co-localization of JMJD7 with  
162 DRG1 and DRG2 in both nuclear and cytoplasmic compartments. Overall, the combined interaction

163 and localization data support the assignment of DRG1 and DRG2 as JMJD7 interactors and potential  
164 substrates.

165

### 166 *JMJD7 catalyzes DRG lysyl hydroxylation*

167 To investigate whether DRG/DFRP complexes are JMJD7 substrates, HA-DRG1/2 and V5-DFRP1/2  
168 were purified from cells overproducing control or FLAG-JMJD7, hydrolyzed by trypsin, then  
169 analyzed by MS. The results identified a single lysyl hydroxylation site in a highly conserved region  
170 in both DRG1 and DRG2, i.e. at K22/K21, respectively (**Fig. 3a-b** and **Supplementary Fig. 10**).  
171 Notably, in cells overexpressing JMJD7, we reproducibly observed increases in hydroxylated peptides  
172 corresponding to a ‘missed’ trypsin cleavage site in DRG1 (NK(OH)ATAHHLGLLK) and DRG2  
173 (NK(OH)ATEYHLGLLK), suggesting that JMJD7-catalyzed hydroxylation hinders trypsin-catalyzed  
174 hydrolysis (**Fig. 3b**).

175

176 We then tested the cellular assignment of JMJD7-mediated DRG1/2 lysyl hydroxylation by assaying  
177 20-mer peptide fragments spanning the DRG1 sequence as substrates (**Supplementary Table 2**; a 25-  
178 mer peptide, DRG1<sub>16-40</sub>, was also used for biochemical characterization as described later in the text).  
179 Consistent with the cell results (**Fig. 3a-b** and **Supplementary Fig. 9**), the only peptide undergoing a  
180 JMJD7-dependent +16 Da shift was DRG1<sub>21-40</sub> (NKATAHHLGLLKARLAKLRR-NH<sub>2</sub>; **Fig. 3c**).  
181 Peptide hydroxylation was impaired by the absence of 2OG and Fe(II) and inhibited by NOG<sup>18</sup> or use  
182 of a JMJD7 H178A variant (**Fig. 3d**). Incubation under <sup>18</sup>O<sub>2</sub> revealed that JMJD7 catalyzes  
183 incorporation of <sup>18</sup>O into its product, as observed for other 2OG protein hydroxylases  
184 (**Supplementary Fig. 11**). Alanine substitution at the hydroxylation site prevented hydroxylation and  
185 blocked interaction between isolated JMJD7 and DRG1/2 (**Supplementary Figs. 12** and **13**).  
186 Interestingly, the DRG-hydroxylation sites are highly conserved in almost all animals including  
187 *Drosophila* (**Fig. 3a**). Recombinant dmJMJD7 hydroxylates human DRG1 and 2 peptides with  
188 similar efficiency as human JMJD7 (**Supplementary Fig. 14a**, compare to **Supplementary Fig. 15**).  
189 Furthermore, dmJMJD7 is able to reconstitute activity-dependent interactions with endogenous DRG1  
190 and DRG2 in human cells (**Supplementary Fig. 14b**). These analyses suggest JMJD7-catalyzed DRG

191 hydroxylation is highly conserved in animals, possibly in a manner linked to the growth phenotype  
192 observed on *dmJMJD7* knockdown in *Drosophila* (**Supplementary Fig. 2**).

193

194 The DRG2 peptide (DRG2<sub>20-39</sub>; NKATEYHLGLLKAKLAKYRA-NH<sub>2</sub>) was a less efficient substrate  
195 than the analogous DRG1<sub>21-40</sub> substrate (**Supplementary Fig. 15a-b**). A structure of the DRG1  
196 homologue from *Saccharomyces cerevisiae* [Ribosome-interacting GTPase 1 (RBG1), 66% sequence  
197 identity, PDB ID: 4A9A] reveals the K22 side-chain protrudes from a loop on a highly conserved  
198 region of a helix-turn-helix (HTH) motif (**Fig. 3a** and **Supplementary Fig. 15c**)<sup>23</sup>. Strikingly, the  
199 position of K22 in the HTH of RBG1, and by implication DRG1/2, resembles that of the lysyl  
200 hydroxylation site of a JMJD4 substrate, eRF1<sup>14</sup> (**Supplementary Fig. 15c-d**). The location of K22  
201 protruding from a turn between 2  $\alpha$ -helices suggests secondary structure may be important in JMJD7-  
202 substrate recognition, as for JMJD4<sup>14</sup>. Increasing the DRG1 fragment length at its *N*-terminus to  
203 include other conserved residues in the HTH (DRG1<sub>16-40</sub>; ARTQKNKATAHHLGLLKARLAKLRR-  
204 NH<sub>2</sub>) results in more efficient hydroxylation (**Supplementary Fig. 15a-b**). Importantly, the *N*-  
205 terminally extended DRG2<sub>15-39</sub> fragment (ARTQKNKATEYHLGLLKAKLAKYRA-NH<sub>2</sub>) undergoes  
206 efficient hydroxylation. To investigate how JMJD7 interacts with DRG1/2, we attempted to obtain  
207 JMJD7.DRG1/2 crystal structures, but have as yet been unsuccessful. We therefore modelled  
208 JMJD7.Fe.2OG.DRG1 complexes based on the crystal structures of JMJD7.Mn.2OG (PDB: 5NFO)  
209 and *S. cerevisiae* RBG1 (PDB: 4A9A). The modelling and cysteine substitution studies  
210 (**Supplementary Fig. 16**) support the combined biochemical observations implying long-range  
211 interactions involving conserved residues distant from those immediately surrounding the  
212 hydroxylated lysine are important in productive JMJD7 binding. Overall, the combined cellular and  
213 isolated protein studies define JMJD7 as a lysyl hydroxylase acting on both DRG1 and DRG2.

214

215 To investigate whether JMJD7 is *necessary* for hydroxylation of DRGs, we immunopurified  
216 endogenous DRG1/2 from HEK293T cells (**Supplementary Fig. 17**); MS analyses identified  
217 substantial levels of both K22 (**Supplementary Fig. 17d**) and K21 (**Fig. 3e-f**) hydroxylation,  
218 respectively. Importantly, endogenous levels of DRG2 K21 hydroxylation depended on the presence

219 of JMJD7 expression (**Fig. 3f** and **Supplementary Fig. 17b**). Consistent with the overexpression  
220 analyses (**Fig. 3b** and **Supplementary Fig. 10**), the ability of trypsin to cleave endogenous DRGs at  
221 the C-terminal side of K22/K21 was reduced following hydroxylation (**Fig. 3f**). We also observed  
222 inhibition of DRG hydrolysis by hydroxylation with Lys-N, which cleaves at the N-terminal side of  
223 lysyl-residues (**Supplementary Fig. 18**). This phenomenon has not been reported following  
224 hydroxylation of lysine at the C4 or C5 positions by protein hydroxylases<sup>14,24,25</sup>, implying JMJD7  
225 catalyzes a novel form of lysyl hydroxylation.

226

### 227 *JMJD7 is a (3S)-lysyl hydroxylase*

228 To date, characterized 2OG oxygenases catalyze hydroxylation at the C4 (e.g. JMJD4<sup>14</sup>) and C5 (e.g.  
229 JMJD6 and the procollagen lysyl hydroxylases (PLODs)<sup>10,26</sup>) positions of lysyl side-chains. To  
230 investigate the regio- and stereo-selectivity of JMJD7, a DRG1 peptide was hydroxylated, then  
231 hydrolyzed and subjected to amino acid analysis. Following derivatization, LC-MS revealed a new  
232 peak, not present in controls, with a mass corresponding to derivatized hydroxylysine (obsvd.  
233 503.2162 Da; calcd. 503.2037 Da). Comparison using C3-, C4-, and C5- hydroxylysine standards<sup>14</sup>  
234 reveals the product co-elutes with one of the C3 hydroxylysine enantiomeric pairs (**Fig. 4a** and  
235 **Supplementary Fig. 19**); C3 hydroxylation is supported by NMR analyses of hydroxylated DRG1  
236 and DRG2 peptides (**Supplementary Fig. 20**). Comparison with a diastereomeric mixture of C3  
237 hydroxylysine isomers and synthetic (2*S*,3*R*)/(2*R*,3*S*)-hydroxylysine standard<sup>27</sup> identified (2*S*,3*S*)-  
238 hydroxylysine as the JMJD7-catalyzed product (**Fig. 4b** and **Supplementary Fig. 19c-d**). No  
239 evidence for other isomers was observed within detection limits, revealing JMJD7 stereospecifically  
240 catalyzes (3*S*)-hydroxylation (**Fig. 4a-c**; assuming retention of (2*S*)-stereochemistry), a previously  
241 undescribed PTM.

242

### 243 *DRG hydroxylation promotes ribonucleic acid binding*

244 The effect of C3 lysyl hydroxylation on *in vitro* proteolysis suggests that this novel PTM can regulate  
245 intramolecular interactions with functional consequences. We therefore explored potential biological  
246 roles of DRG C3 lysyl hydroxylation. Unlike HIF hydroxylases, JMJD7 did not significantly regulate

247 substrate levels: Overexpression of wildtype or H178A JMJD7 (**Fig. 2a** and **Supplementary Fig. 9b-**  
248 **d**), treatment with DMOG (**Supplementary Fig. 9b-d**), or DRG hydroxylation site mutation  
249 (**Supplementary Figs 21** and **22**) did not consistently affect the expression of DRG or DFRP proteins  
250 in cells. Furthermore, hydroxylation did not, within detection limits, change the thermal stability of  
251 full-length, isolated DRG1 (using differential scanning calorimetry; **Supplementary Fig. 23**).  
252 Consistent with a lack of effect on cellular stability, hydroxylation site substituted DRGs did not  
253 affect their ability to co-precipitate DFRPs, which are major regulators of DRG protein turnover<sup>22</sup>  
254 (**Supplementary Fig. 21**). Hydroxylation also did not consistently affect GTPase activity, as  
255 determined by <sup>1</sup>H NMR or phosphate release assays using recombinant DRG1 *in vitro*  
256 (**Supplementary Fig. 24**), or using DRG1/2 purified from cells exposed to JMJD7 overexpression,  
257 shRNA knockdown, or DMOG treatment (**Supplementary Fig. 25**).

258

259 As described above, the lysine residue targeted by JMJD7 is located at the apex of a highly conserved  
260 HTH motif within the *N*-terminal regions of DRG1/2 (**Supplementary Fig. 15c**). Although the role of  
261 this domain has not previously been reported, yeast complementation studies reveal it is critical for  
262 DRG function<sup>28</sup>. JMJD7-mediated DRG hydroxylation is analogous to JMJD4-mediated eRF1  
263 hydroxylation (**Supplementary Fig. 15c-d**), in the sense that both are lysyl hydroxylation events  
264 targeting HTH domains. eRF1 lysyl hydroxylation is thought to promote translation termination by  
265 supporting the interaction of eRF1 with the mRNA stop codon<sup>14</sup>, raising the possibility that DRG  
266 lysyl hydroxylation catalyzed by JMJD7 has a related function. Indeed, we observed significant  
267 binding of DRG2 to RNA affinity columns (**Supplementary Fig. 22**; consistent with previous  
268 reports<sup>29</sup>). Furthermore, a DRG2 K21 mutant had reduced affinity, thus localizing RNA binding  
269 activity to the HTH domain (**Supplementary Fig. 22**). Importantly, shRNA-mediated JMJD7  
270 knockdown also reduced the RNA binding affinity of purified DRG2 (**Fig. 4d** and **Supplementary**  
271 **Fig. 22d**). These data support a role for JMJD7-mediated C3 lysyl hydroxylation in promoting the  
272 interaction of the DRG TRAFAC GTPases with RNA. Future work can focus on defining the precise  
273 nature of the JMJD7-DRG-DFRP ribonucleoprotein complexes and their biological roles.

274

275 **DISCUSSION**

276 The combined cellular and biochemical results demonstrate that JMJD7 targets highly conserved  
277 lysine residues within 2 closely related TRAFAC GTPase proteins. The finding that JMJD7 catalyzes  
278 (3*S*)-lysyl hydroxylation, the first time this PTM has been observed in humans, expands the repertoire  
279 of 2OG oxygenase-catalyzed modifications of basic residues, which also include histidinyl-  
280 hydroxylation<sup>12,30</sup>, lysyl C4 hydroxylation<sup>14</sup>, lysyl (5*S*)- and (5*R*)-hydroxylation<sup>24,26</sup>, N<sup>ε</sup>-methyl lysyl  
281 demethylation<sup>31</sup>, argininy C3 hydroxylation<sup>12</sup> and, possibly, N-methyl argininy demethylation<sup>32</sup>. The  
282 extent of 2OG oxygenase-catalyzed lysyl hydroxylation is striking. With the discovery of JMJD7-  
283 catalyzed C3 lysyl hydroxylation, a total of seven different lysine residues oxidations are now known  
284 to be catalyzed by 2OG oxygenases. Aside from the ‘not (yet) observed’ C3 and C4 stereoisomers,  
285 oxidation at the C2 and C6 positions are unidentified exceptions; although the products of such  
286 reactions are likely unstable, they have precedent in 2OG oxygenase catalyzed protein fragmentation  
287 (albeit not at lysine residues as yet) via C2 hydroxylation<sup>33</sup>.

288

289 In most cases, the detailed biochemical roles of lysyl hydroxylations are unclear, with the enablement  
290 of glycosylation by procollagen (5*R*)-lysyl hydroxylation<sup>26</sup> and improved stop codon decoding by C4  
291 lysyl hydroxylation<sup>14,34,35</sup> being exceptions. Our experiments indicate that JMJD7-catalyzed  
292 hydroxylation does not substantially effect on the intrinsic stability, protein expression, or GTPase  
293 activity of DRGs. Interestingly, however, we observed that JMJD7-catalyzed C3 lysyl hydroxylation  
294 clearly impairs experimental proteolysis, at either the C- or N-terminal sides of the target lysyl-  
295 residue. While inhibition of the tested proteases is likely not biologically relevant, this observation  
296 raises the possibility of a wider role for protein hydroxylation in directly modulating protease  
297 hydrolysis. This is particularly attractive for C3 lysyl-hydroxylation and nucleophilic serine/threonine  
298 protease inhibition, where work with proteases and bacterial cell wall biosynthesis enzymes  
299 employing nucleophilic serine catalysis has revealed that substrate/inhibitor substitutions that perturb  
300 hydrolysis (or formation) of the acyl-enzyme complex can lead to inhibition<sup>36</sup>.

301

302 In addition to effects on protease hydrolysis, we observed JMJD7- and hydroxylation site-dependent  
303 regulation of RNA binding, analogous to the role of JMJD4 in promoting mRNA stop codon decoding  
304 by eRF1<sup>14</sup>. Although future work is required to address the physiological RNA targets, the presence of  
305 DRGs in ribosome fractions from diverse species including yeasts, plants, and humans<sup>28,37,38</sup> could be  
306 consistent with an interaction with messenger or ribosomal RNA. Although the biochemical role of  
307 the DRGs in protein translation is unclear, it is consistent with their similarity to other OBG GTPases  
308 of the TRAFAC family, which have roles in ribosome biogenesis and translation control<sup>23,39</sup>. A  
309 prokaryotic 2OG-dependent prolyl hydroxylase homologous with the animal HIF prolyl hydroxylases,  
310 Elongation Factor Thermo unstable (EF-Tu), has also been found to catalyze hydroxylation of a loop  
311 region of a translation-associated GTPase<sup>40</sup>; thus, physical and functional interactions between 2OG  
312 oxygenases, translation factors, and RNA may have ancient origins.

313

314 The discovery of JMJD7-catalyzed DRG hydroxylation contributes to growing evidence on the  
315 importance of the dynamic interactions between 2OG oxygenases and their substrates/interacting  
316 partners in disease<sup>6,41</sup>. Both JMJD7 and DRG1/DRG2 are linked to cell growth in diverse cell types  
317 and species<sup>29,37,42-44</sup>. JMJD7 and DRG1/2 may also have context dependent roles in diseases  
318 including cancer and mental disorders; the *DRG2* gene is located in a chromosomal region implicated  
319 in the Smith-Magenis neurobehavioral syndrome<sup>45</sup>, and DRG1/2 SNPs have been identified in a  
320 screen of candidate genes for autism spectrum disorders<sup>46</sup>. In support of this, genetic studies in high-  
321 risk autism families and persons with severe intellectual disabilities have identified 2 substitutions in  
322 the *JMJD7* gene<sup>20,47</sup>. Future work can now address whether JMJD7-catalyzed hydroxylation of  
323 DRG1/2 regulates protein synthesis and how this underlies the role of this novel pathway in growth  
324 control and disease.

325

## 326 **ACKNOWLEDGEMENTS**

327 We thank the Biotechnology and Biological Sciences Research Council (BB/L009846/1, CJS),  
328 Medical Research Council (MR/N021053/1, MLC), Wellcome Trust (106244/Z/14/Z, CJS), Cancer  
329 Research UK (24552, MLC), University of Oxford Clarendon Fund (SM), and a Junior Research

330 Fellowship from Kellogg College, University of Oxford (MIA) for support. We thank E Flashman  
331 (Department of Chemistry, University of Oxford) for assistance with the <sup>18</sup>O<sub>2</sub> experiment and K  
332 Connolly (Institute of Cancer and Genomics Sciences, University of Birmingham) for *Drosophila*  
333 cDNA.

334

#### 335 **AUTHOR CONTRIBUTIONS:**

336 S.M., Q.Z., S.E.W., M.J.K., P.W., R.C., M.L.C, and C.J.S. designed and conceived the research; S.M.  
337 prepared recombinant proteins; Q.Z. performed substrate discovery proteomics; S.M. performed and  
338 analyzed CD spectra and all enzyme activity assays by MALDI-MS and NMR; Q.Z. performed  
339 enzyme:substrate interaction assays; S.M. and R.C. performed the crystallography in which R.C.  
340 played both an experimental and supervisory role; C.E. performed confocal microscopy, cellular  
341 dimerization, and dmJMJD7 interaction experiments; Q.Z., C.H., and H.E.M. prepared mammalian  
342 expression constructs used by Q.Z.; W.G. and S.M. prepared plasmids for recombinant protein  
343 production; S.M. performed / analyzed amino acid analyses with guidance from S.E.W; M.I.A.  
344 performed and analyzed peptide NMR work; Q.Z. purified exogenous and endogenous proteins for  
345 MS / analyzed data with help from M.L.C; M.I.A. produced and purified recombinant DRG1,  
346 performed DRG1 stability and activity assays, and analyzed data; R.K., S.D., and R.F. performed MS  
347 (B.M.K.) and analyzed data; Q.Z. performed all JMJD7 loss-of-function experiments and DRG/DFRP  
348 interaction, GTPase, and RNA binding assays; R.K.L. prepared hydroxylysine standards; S.M. and  
349 W.B.S. performed and analyzed native MS / SEC-MALS (J.L.B.); M.J.K. and P.W. performed and  
350 analyzed *Drosophila* experiments; R.C. performed enzyme:substrate modelling, prepared recombinant  
351 dmJMJD7, and performed proteolysis assays; M.Y., M.E.C., and P.J.R. performed preliminary  
352 immunoprecipitations; S.M., Q.Z., S.E.W., C.E., R.C., M.L.C., and C.J.S. analyzed data; S.M., Q.Z.,  
353 R.C., M.L.C., and C.J.S. wrote the manuscript.

354

#### 355 **COMPETING INTERESTS**

356 The authors declare no competing interests.

357

358 **REFERENCES**

- 359 1. Markolovic, S., Wilkins, S. E. & Schofield, C. J. Protein hydroxylation catalyzed by 2-  
360 oxoglutarate-dependent oxygenases. *J. Biol. Chem.* **290**, 20712–20722 (2015).
- 361 2. Ploumakis, A. & Coleman, M. L. OH, the places you'll go! Hydroxylation, gene expression,  
362 and cancer. *Mol. Cell* **58**, 729–741 (2015).
- 363 3. Semenza, G. L. Oxygen sensing, hypoxia-inducible factors, and disease pathophysiology.  
364 *Annu. Rev. Pathol.* **9**, 47–71 (2014).
- 365 4. Elkins, J. M. *et al.* Structure of factor-inhibiting hypoxia-inducible factor (HIF) reveals  
366 mechanism of oxidative modification of HIF-1 $\alpha$ . *J. Biol. Chem.* **278**, 1802–1806 (2003).
- 367 5. Walport, L. J., Hopkinson, R. J. & Schofield, C. J. Mechanisms of human histone and nucleic  
368 acid demethylases. *Curr. Opin. Chem. Biol.* **16**, 525–534 (2012).
- 369 6. Johansson, C. *et al.* The roles of Jumonji-type oxygenases in human disease. *Epigenomics* **6**,  
370 89–120 (2014).
- 371 7. Morera, L., Lübbert, M. & Jung, M. Targeting histone methyltransferases and demethylases in  
372 clinical trials for cancer therapy. *Clin. Epigenetics* **8**, 57 (2016).
- 373 8. Chan, M. C., Holt-Martyn, J. P., Schofield, C. J. & Ratcliffe, P. J. Pharmacological targeting  
374 of the HIF hydroxylases – A new field in medicine development. *Mol. Aspects Med.* **47–48**,  
375 54–75 (2016).
- 376 9. Cockman, M. E., Webb, J. D. & Ratcliffe, P. J. FIH-dependent asparaginyl hydroxylation of  
377 ankyrin repeat domain-containing proteins. *Ann. N. Y. Acad. Sci.* **1177**, 9–18 (2009).
- 378 10. Webby, C. J. *et al.* Jmjd6 catalyses lysyl-hydroxylation of U2AF65, a protein associated with  
379 RNA splicing. *Science* **325**, 90–93 (2009).
- 380 11. Chowdhury, R. *et al.* Ribosomal oxygenases are structurally conserved from prokaryotes to  
381 humans. *Nature* **510**, 422–426 (2014).
- 382 12. Ge, W. *et al.* Oxygenase-catalyzed ribosome hydroxylation occurs in prokaryotes and humans.  
383 *Nat. Chem. Biol.* **8**, 960–962 (2012).
- 384 13. Kato, M. *et al.* Crystal structure of a novel JmjC-domain-containing protein, TYW5, involved  
385 in tRNA modification. *Nucleic Acids Res.* **39**, 1576–1585 (2011).

- 386 14. Feng, T. *et al.* Optimal translational termination requires C4 lysyl hydroxylation of eRF1. *Mol.*  
387 *Cell* **53**, 645–654 (2014).
- 388 15. Zhuang, Q., Feng, T. & Coleman, M. L. Modifying the maker: Oxygenases target ribosome  
389 biology. *Transl.* **3**, e1009331 (2015).
- 390 16. Del Rizzo, P. A., Krishnan, S. & Trievel, R. C. Crystal structure and functional analysis of  
391 JMJD5 indicate an alternate specificity and function. *Mol. Cell. Biol.* **32**, 4044–4052 (2012).
- 392 17. Markolovic, S. *et al.* Structure–function relationships of human JmjC oxygenases—  
393 demethylases versus hydroxylases. *Curr. Opin. Struct. Biol.* **41**, 62–72 (2016).
- 394 18. Rose, N. R., McDonough, M. A., King, O. N. F., Kawamura, A. & Schofield, C. J. Inhibition  
395 of 2-oxoglutarate dependent oxygenases. *Chem. Soc. Rev.* **40**, 4364–4397 (2011).
- 396 19. Kandoth, C. *et al.* Integrated genomic characterization of endometrial carcinoma. *Nature* **497**,  
397 67–73 (2013).
- 398 20. Matsunami, N. *et al.* Identification of rare DNA sequence variants in high-risk autism families  
399 and their prevalence in a large case/control population. *Mol. Autism* **5**, 5 (2014).
- 400 21. Lancaster, D. E. *et al.* Disruption of dimerization and substrate phosphorylation inhibit factor  
401 inhibiting hypoxia-inducible factor (FIH) activity. *Biochem. J.* **383**, 429–437 (2004).
- 402 22. Ishikawa, K., Azuma, S., Ikawa, S., Semba, K. & Inoue, J. I. Identification of DRG family  
403 regulatory proteins (DFRPs): Specific regulation of DRG1 and DRG2. *Genes to Cells* **10**, 139–  
404 150 (2005).
- 405 23. Francis, S. M., Gas, M.-E., Daugeron, M.-C., Bravo, J. & Seraphin, B. Rbg1-Tma46 dimer  
406 structure reveals new functional domains and their role in polysome recruitment. *Nucleic Acids*  
407 *Res.* **40**, 11100–11114 (2012).
- 408 24. Mantri, M. *et al.* The 2-oxoglutarate-dependent oxygenase JMJD6 catalyses oxidation of  
409 lysine residues to give 5S-hydroxylysine residues. *ChemBioChem* **12**, 531–534 (2011).
- 410 25. Witkop, B. The application of Hudson’s lactone rule to  $\gamma$ - and  $\delta$ -hydroxyamino acids and the  
411 question of the configuration of  $\delta$ -hydroxy-L-lysine from collagen. *Experientia* **XII**, 372–374  
412 (1956).
- 413 26. Myllyharju, J. & Kivirikko, K. I. Collagens and collagen-related diseases. *Ann. Med.* **33**, 7–21

- 414 (2001).
- 415 27. Leśniak, R. K., Markolovic, S., Tars, K. & Schofield, C. J. Human carnitine biosynthesis  
416 proceeds via (2*S*,3*S*)-3-hydroxy- $N^{\epsilon}$ -trimethyllysine. *Chem. Commun.* **53**, 440–442 (2017).
- 417 28. Daugeron, M.-C., Prouteau, M., Lacroute, F. & Séraphin, B. The highly conserved eukaryotic  
418 DRG factors are required for efficient translation in a manner redundant with the putative  
419 RNA helicase Slh1. *Nucleic Acids Res.* **39**, 2221–2233 (2011).
- 420 29. Ishikawa, K. *et al.* Cloning and characterization of *Xenopus laevis* drg2, a member of the  
421 developmentally regulated GTP-binding protein subfamily. *Gene* **322**, 105–112 (2003).
- 422 30. Yang, M. *et al.* Factor-inhibiting hypoxia-inducible factor (FIH) catalyses the post-  
423 translational hydroxylation of histidiny residues within ankyrin repeat domains. *FEBS J.* **278**,  
424 1086–1097 (2011).
- 425 31. Klose, R. J., Kallin, E. M. & Zhang, Y. JmjC-domain-containing proteins and histone  
426 demethylation. *Nat. Rev. Genet.* **7**, 715–727 (2006).
- 427 32. Walport, L. J. *et al.* Arginine demethylation is catalysed by a subset of JmjC histone lysine  
428 demethylases. *Nat. Commun.* **7**, 11974 (2016).
- 429 33. Mantri, M., Zhang, Z., McDonough, M. A. & Schofield, C. J. Autocatalysed oxidative  
430 modifications to 2-oxoglutarate dependent oxygenases. *FEBS J.* **279**, 1563–1575 (2012).
- 431 34. Matheisl, S., Berninghausen, O., Becker, T. & Beckmann, R. Structure of a human translation  
432 termination complex. *Nucleic Acids Res.* **43**, 8615–8626 (2015).
- 433 35. Brown, A., Shao, S., Murray, J., Hegde, R. S. & Ramakrishnan, V. Structural basis for stop  
434 codon recognition in eukaryotes. *Nature* **524**, 493–496 (2015).
- 435 36. Powers, J. C., Asgian, J. L., Ekici, O. D. & James, K. E. Irreversible inhibitors of serine,  
436 cysteine, and threonine proteases. *Chem. Rev.* **102**, 4639–4750 (2002).
- 437 37. Nelson, B. J., Maas, K. J., Dekeyser, J. L. & Stafstrom, J. P. Association of DRG1 and DRG2  
438 with ribosomes from pea, arabidopsis, and yeast. *Int. J. Plant Sci.* **170**, 834–844 (2009).
- 439 38. Ishikawa, K., Akiyama, T., Ito, K., Semba, K. & Inoue, J. Independent stabilizations of  
440 polysomal Drg1/Dfrp1 complex and non-polysomal Drg2/Dfrp2 complex in mammalian cells.  
441 *Biochem. Biophys. Res. Commun.* **390**, 552–556 (2009).

- 442 39. Leipe, D. D., Wolf, Y. I., Koonin, E. V. & Aravind, L. Classification and evolution of P-loop  
443 GTPases and related ATPases. *J. Mol. Biol.* **317**, 41–72 (2002).
- 444 40. Scotti, J. S. *et al.* Human oxygen sensing may have origins in prokaryotic elongation factor Tu  
445 prolyl-hydroxylation. *Proc. Natl. Acad. Sci.* **111**, 13331–13336 (2014).
- 446 41. *2-Oxoglutarate-dependent oxygenases. RSC Metallobiology Series No. 3* (Royal Society of  
447 Chemistry, 2015).
- 448 42. Jang, S. H., Kim, A.-R., Park, N.-H., Park, J. W. & Han, I.-S. DRG2 regulates G2/M  
449 progression via the cyclin B1-Cdk1 complex. *Mol. Cells* **39**, 699–704 (2016).
- 450 43. Lu, L., Lv, Y., Dong, J., Hu, S. & Peng, R. DRG1 is a potential oncogene in lung  
451 adenocarcinoma and promotes tumor progression via spindle checkpoint signaling regulation.  
452 *Oncotarget* **7**, 72795–72806 (2016).
- 453 44. Wei, D. *et al.* Molecular cloning and expression of two closely related GTP-binding proteins  
454 from zebrafish. *DNA Seq.* **15**, 246–250 (2004).
- 455 45. Vlangos, C. N., Das, P., Patel, P. I. & Elsea, S. H. Assignment of developmentally regulated  
456 GTP-binding protein (DRG2) to human chromosome band 17p11.2 with somatic cell hybrids  
457 and localization to the Smith-Magenis syndrome critical interval. *Cytogenet. Cell Genet.* **88**,  
458 283–285 (2000).
- 459 46. de Krom, M. *et al.* A common variant in DRD3 receptor is associated with autism spectrum  
460 disorder. *Biol. Psychiatry* **65**, 625–630 (2009).
- 461 47. de Ligt, J. *et al.* Diagnostic exome sequencing in persons with severe intellectual disability. *N.*  
462 *Engl. J. Med.* **367**, 1921–1929 (2012).
- 463

464 **FIGURE LEGENDS**

465 **Figure 1. Structural analyses of the JmjC hydroxylase, JMJD7.** (a) View from a crystal structure  
466 of human JMJD7 complexed with Mn(II) (violet sphere) and 2OG (yellow) showing the unique  
467 dimerization interface, which involves regions both *N*- and *C*-terminal to the double-stranded  $\beta$ -helix  
468 (DSBH) core fold and the disulfide between Cys47 of each monomer (\*, red).  $\beta$ -Strands comprising  
469 the distorted 8-stranded (I-VIII) DSBH, conserved in 2OG oxygenases, are in salmon. (b) At the  
470 active site, Mn (substituting for Fe(II), violet sphere) is octahedrally coordinated by H178, D180,  
471 H277, the 2OG oxalyl group (yellow), and water (red sphere). 2OG is apparently tightly bound by  
472 hydrogen bonding/electrostatic interactions between its C5 carboxylate and Y127, T175, Y186, and  
473 K193, and its C1 carboxylate with N184 and N289 (dotted lines, numerical values represent H-bond  
474 distances in Å).

475

476 **Figure 2. JMJD7 interacts with DRG/DFRP complexes in an active site dependent manner.** (a)  
477 Interaction of JMJD7 and DRG/DFRP is consistent with proteomic analyses (**Supplementary Fig.**  
478 **9a**). 3x-FLAG wildtype or inactive (H178A) JMJD7 were produced in doxycycline-inducible  
479 HEK293T cells before anti-FLAG immunopurification (IP) and western blotting with the indicated  
480 antibodies. Note the lack of interaction of DRG and DFRP proteins with JMJD7 H178A. The  
481 specificity of endogenous DRG antibodies was verified by siRNA knockdown (**Supplementary Fig.**  
482 **9f**). Immunoprecipitation experiments validating proteomic data were repeated three times, with  
483 similar results. Uncropped western blots are provided in Supplementary Figure 27. (b) Endogenous  
484 DRG/DFRP complexes contain endogenous JMJD7. Endogenous DFRP1 (left) or DFRP2 (right)  
485 complexes were immunopurified from HEK293T cells prior to western blotting with the indicated  
486 antibodies. Note that immunoprecipitation samples were diluted 1:10 prior to analyses of ‘bait’  
487 (DFRP/DRG levels). This interaction experiment was repeated three times, with similar results.  
488 Uncropped western blots are provided in Supplementary Figure 28. (c) Co-localization of DRG1/2  
489 and JMJD7. HeLa cells were transfected with control (empty vector, EV), FLAG-JMJD7 and/or HA-

490 DRG1/2 prior to immunostaining for HA (red) and JMJD7 (green) and labeling nuclei with DAPI.  
491 This experiment was repeated three times, with similar results.

492

493 **Figure 3. JMJD7 catalyzes lysyl-hydroxylation of the DRG1/2 GTPases.** (a) Alignment of the  
494 conserved DRG1/2 sequences hydroxylated by JMJD7 in different eukaryotes (Protein BLAST; figure  
495 was made using Clustal Omega and GeneDoc). (b) Qualitative analysis of the extent of (upper)  
496 DRG1 K22 and (lower) DRG2 K21 hydroxylation in the (left) absence or (right) presence of JMJD7  
497 overexpression. Trypsinolysis at K22 of DRG1 and K21 of DRG2 is impeded by hydroxylation,  
498 complicating quantification: precursor signal intensities of the indicated tryptic fragments, as judged  
499 by precursor ion chromatogram analysis, were used; a shift in proportion of the fully-trypsinized  
500 peptide signal to the uncleaved trypsinized lysyl-hydroxylated peptide signal is indicative of increased  
501 hydroxylation. See **Supplementary Fig. 10** for MS/MS fragments detected. (c) Representative  
502 MALDI mass spectra for (left) wildtype DRG1<sub>21-40</sub> and (right) K22A DRG1<sub>21-40</sub> in the absence (black)  
503 or presence (orange) of JMJD7. The K22A substitution nearly ablates peptide hydroxylation. This  
504 experiment was repeated three times, with similar results. (d) Representative MALDI-MS assays with  
505 DRG1<sub>16-40</sub> in presence/absence of co-factors/substrates and inhibitor. Ascorbate has no effect on  
506 JMJD7 activity in the linear range (the activity of some 2OG oxygenases is promoted by ascorbate<sup>18</sup>).  
507 The JMJD7-H178A mutant has reduced activity. Data represent the mean  $\pm$  standard deviation (n = 3  
508 replicates with a single biological sample) after incubation for 5 min at 37°C. This assay was repeated  
509 twice, with similar results. (e) MS/MS spectra of the K21 hydroxylated tryptic peptide fragment from  
510 endogenous DRG2 (see **Supplementary Fig17a-c** for extended data, and **Supplementary Fig. 17d-f**  
511 for DRG1). Note that fragments of the hydroxylated peptide lose water (-18 Da, likely to give a  
512 C2/C3 dehydro- species, consistent with C3 hydroxylation), so most b-ions appear as pairs. Similar  
513 spectra were identified in multiple samples from two independent experiments. (f) Quantification of  
514 endogenous DRG2 K21 hydroxylation following control or JMJD7 siRNA. This experiment was  
515 repeated twice, with similar results.

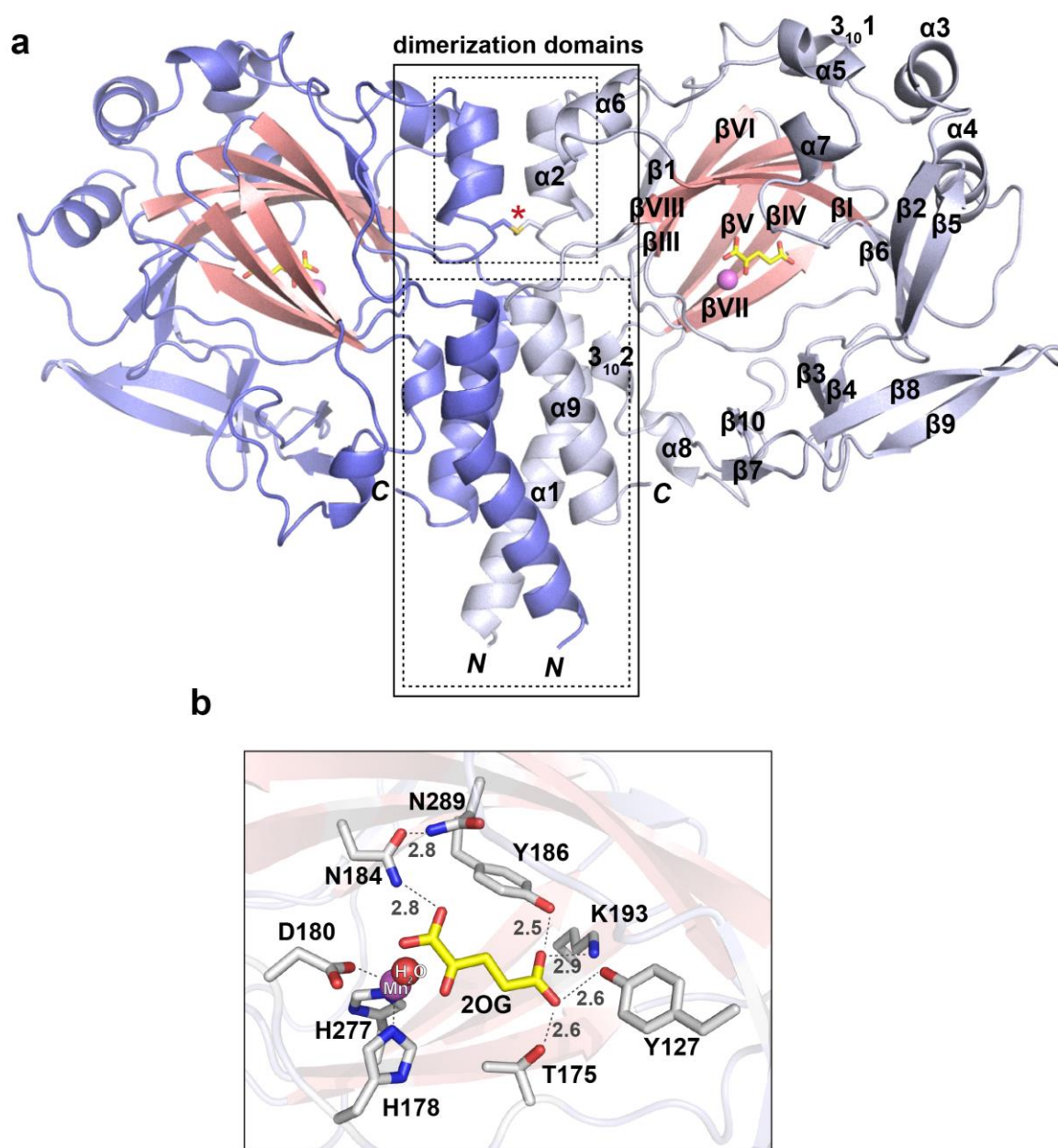
516

517 **Figure 4. JMJD7 is a (3S)-lysyl hydroxylase that promotes DRG ribonucleic acid binding. (a)**  
518 Overlaid extracted ion chromatograms (XIC;  $m/z = 503.2$ ) corresponding to: (i) C3 (dark blue), C4  
519 (light blue), and C5 (cyan) hydroxylysine standards post-derivatization (two peaks are observed  
520 because each standard is a mixture of stereoisomers -  $(2S,XR)/(2R,XS)$  and  $(2S,XS)/(2R,XR)$ ; X is the  
521 hydroxylation site, see **Supplementary Fig. 19**); (ii) hydrolyzed DRG<sub>121-40</sub> peptide incubated with  
522 (orange) or without (black) JMJD7 prior to hydrolysis. The new product in the JMJD7-treated sample  
523 (orange) elutes at the same retention time as one of the C3 stereoisomeric pairs (C3'). (b) Overlaid  
524 XIC ( $m/z = 503.2$ ) corresponding to: (i) C3 hydroxylysine standard sample (dark blue) and  
525  $(2S,3R)/(2R,3S)$ -3-hydroxylysine standard (red) indicates the  $(2S,3R)/(2R,3S)$ -3-hydroxylysine  
526 enantiomeric pair co-elutes with the first peak of the C3 standard; (ii) hydrolyzed DRG<sub>121-40</sub> peptide  
527 incubated with (orange) or without (black) JMJD7. The new peak in JMJD7-sample (orange) elutes at  
528 the same retention time as the standard corresponding to  $(2S,3S)/(2R,3R)$ -3-hydroxylysine (see  
529 **Supplementary Fig. 19**). Amino acid analyses were repeated two or three times, with similar results.  
530 (c) Currently described forms of lysyl hydroxylation and their functions. (d) JMJD7 knockdown  
531 reduces the affinity of purified DRG2 for an RNA poly-C (cytidine nucleotide) agarose column. 3x-  
532 FLAG DRG2 was purified from doxycycline-inducible control shRNA cells (shCON) or two  
533 independent JMJD7 shRNA cell lines (#2 and #3) before anti-FLAG purification and incubation with  
534 poly-C agarose. Captured FLAG-DRG2 was detected by anti-FLAG western blotting (right;  
535 uncropped western blots are provided in Supplementary Figure 39) and quantified in three  
536 independent experiments, with similar results (left): Data represent the mean  $\pm$  s.e.m. (n=3  
537 biologically independent experiments) analyzed by 2-sided students t-test (\*\*  $P < 0.01$ ;  $P = 0.0016$   
538 shJMJD7#2 and 0.0082 shJMJD7#3).

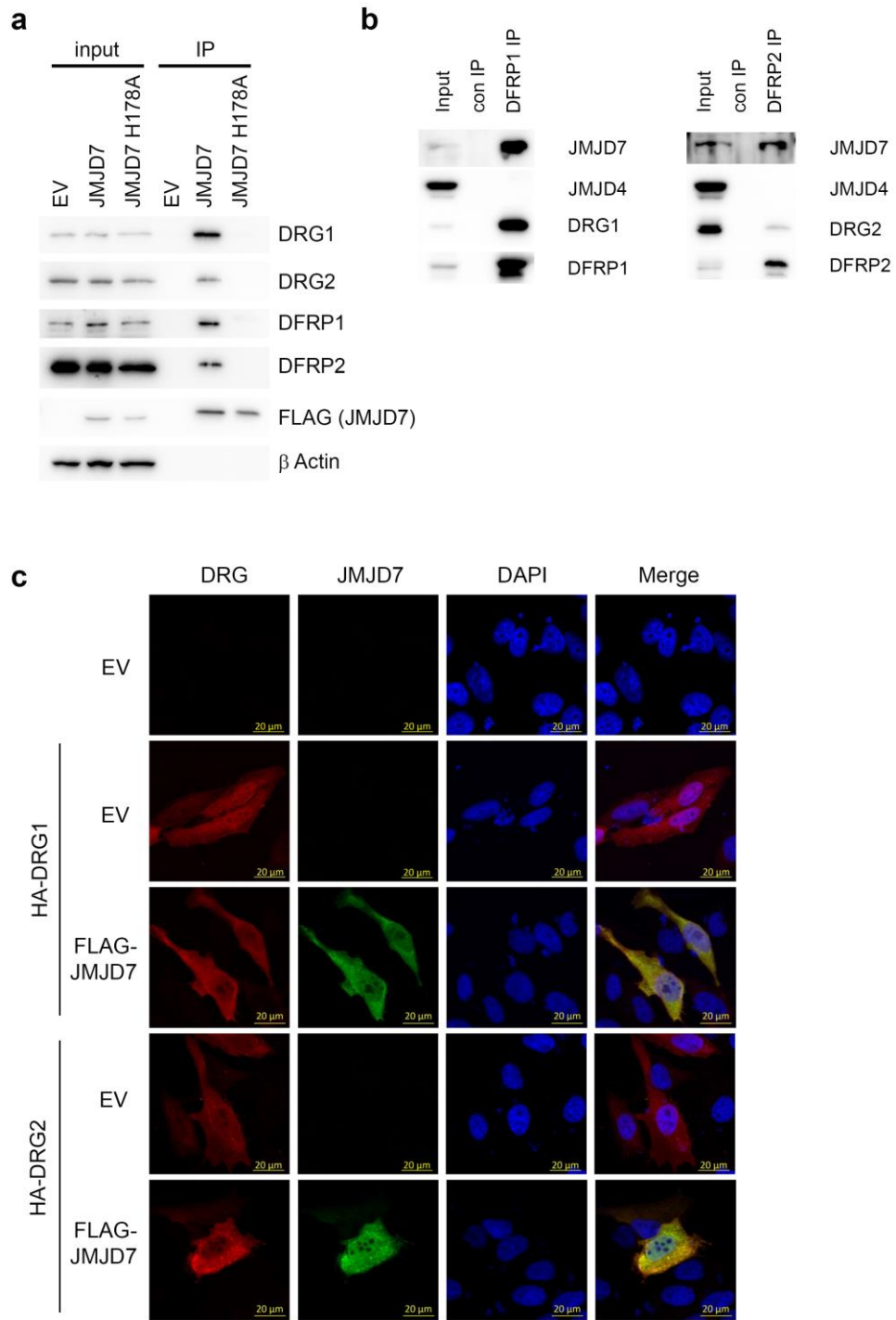
539

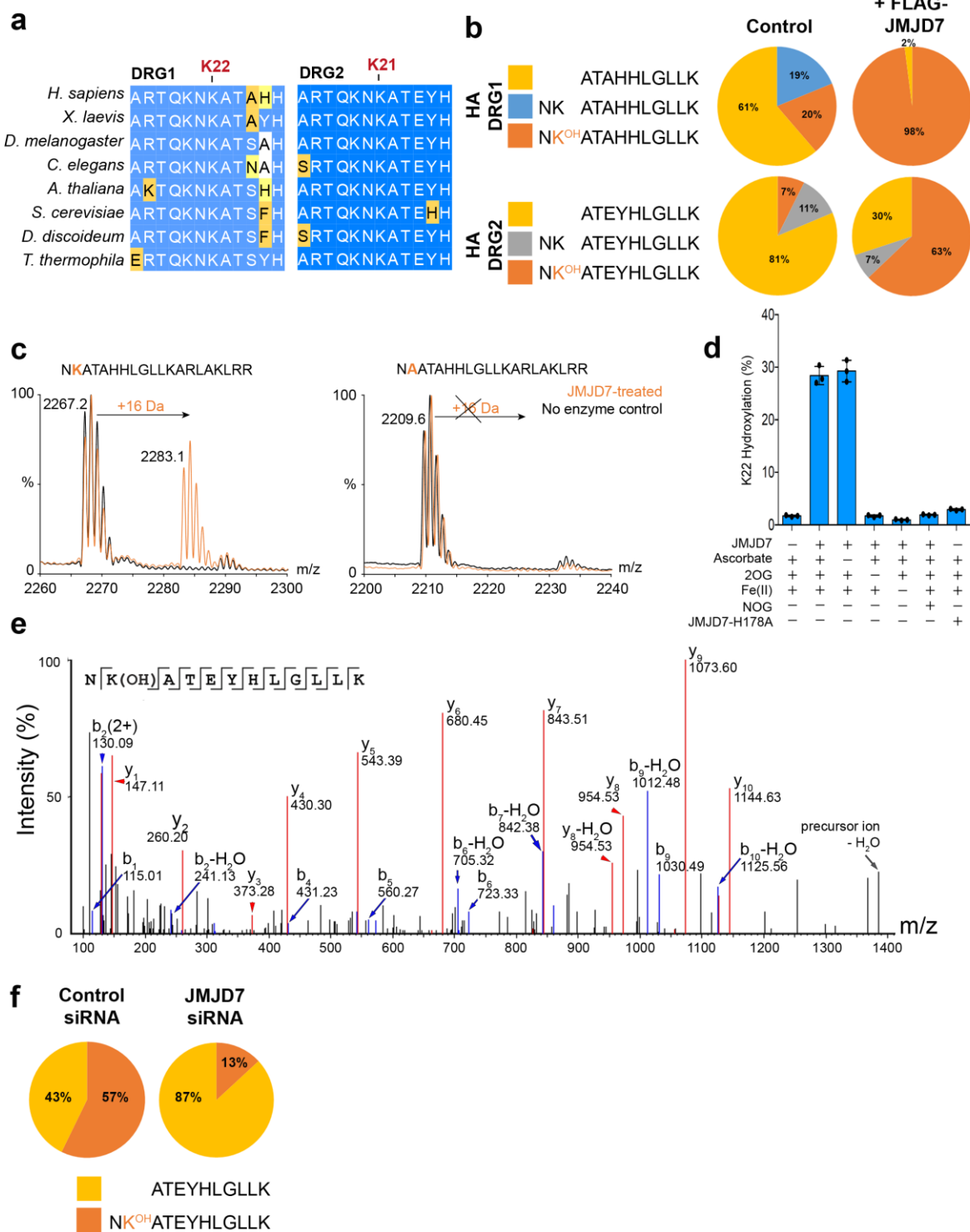
540 FIGURES

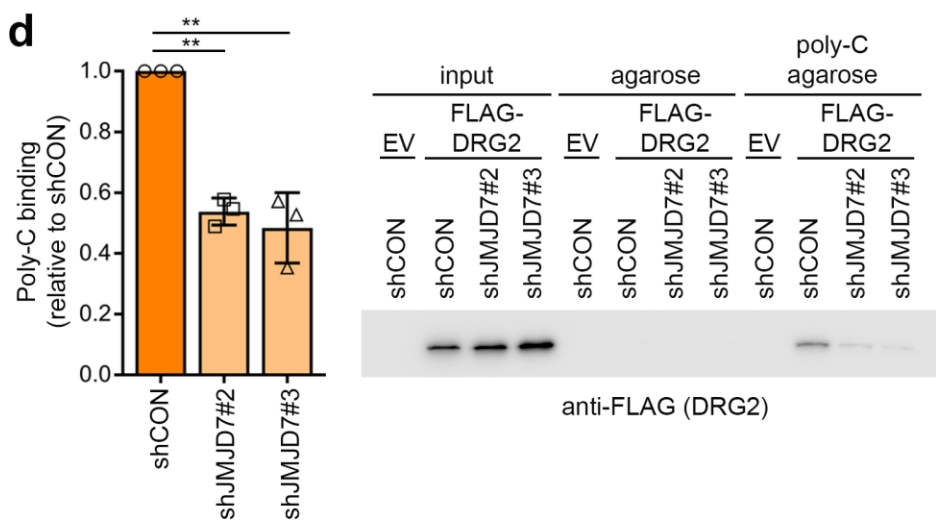
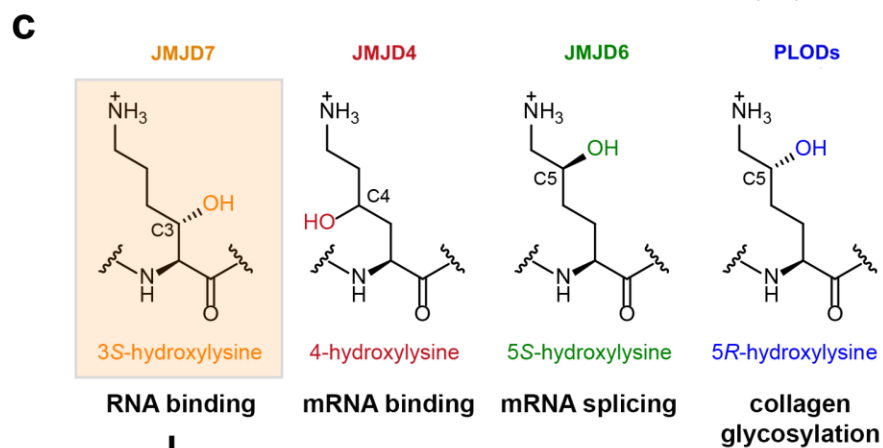
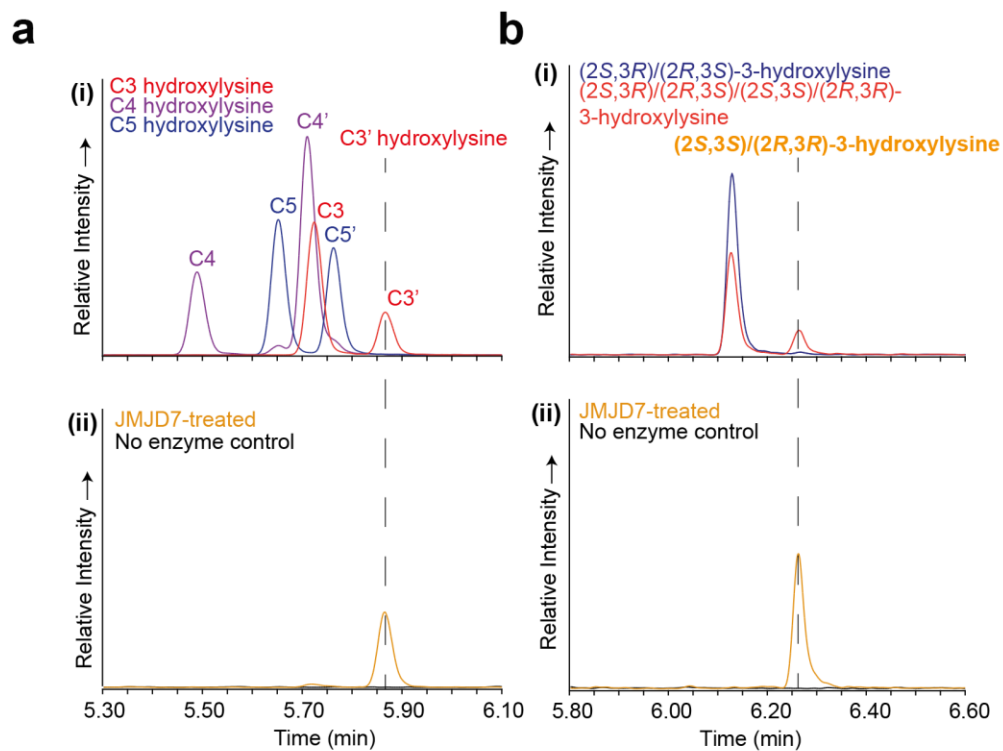
541 FIGURE 1



542  
543







551 **ONLINE METHODS**

552 **Analysis of growth phenotypes in *Drosophila melanogaster***

553 *Drosophila* maintenance, engineering, and knockdowns were performed as described<sup>48</sup>. Flies used in  
554 this study were en-Gal4 from the Bloomington *Drosophila* stock center and white RNAi (as a control)  
555 and *CG10133* RNAi from the VDRC stock center. For analysis of growth phenotypes, wings from 4  
556 day old females and males were removed and mounted in a solution containing 1:1 lactic acid/ethanol.  
557 Wings were imaged using an Olympus MVX10 stereomicroscope connected to an Olympus DP71  
558 digital camera, and variations in the area of the posterior compartment were estimated by measuring  
559 the area comprised between veins L4, PCV and L5, using the ImageJ software (NIH, USA). To  
560 quantify variations of cell size, the number of wing hairs per square mm was counted from images  
561 taken with an Olympus BX60 microscope connected to an Olympus DP71 digital camera.

562

563 **Mammalian cell culture and transfection**

564 Human tumor and HEK293T cell lines were cultured in DMEM supplemented with 10% FBS  
565 (Sigma) and 1% penicillin-streptomycin at 37°C in a humidified atmosphere with 5% CO<sub>2</sub>. Plasmids  
566 were transfected using FuGENE6 Transfection Reagent (Promega) according to manufacturer's  
567 instructions. siRNA oligonucleotides (Sigma MISSION) were transfected twice over consecutive days  
568 at a concentration of 25 nM using OligoFectamine (ThermoFisher), according to the manufacturer's  
569 instructions. Lentiviral particles containing doxycycline-inducible cDNA expression and shRNA  
570 vectors were generated by co-transfection of HEK293T cells with 2<sup>nd</sup> generation vectors (pMD2.G  
571 and psPAX2) and used to create puromycin-resistant stable lines in HeLa, HEK293T, A549 and  
572 SW620 cells. Doxycycline-inducible control and JMJD7 shRNA lentiviral vectors were from the  
573 pZIP-TRE3G shERWOOD Ultramir collection and purchased from Transomic.

574

575 **Statistics, Reagents, and Animal Models**

576 Validated antibodies used in this study included those raised against HA-tag (BioLegend, clone  
577 16B12), DRG1 (Proteintech, 13190-1-AP), DRG2 (Proteintech, 14743-1-AP), JMJD7 (St Johns  
578 Laboratory, STJ29545), JMJD4 (Ximbio, 152745), DFRP1 (SIGMA, HPA031099), DFRP2

579 (GeneTex, GTX120331),  $\beta$ -actin (Abcam, ab8227), FLAG (SIGMA, A8592), and V5 (BioRad,  
580 MCA1360P). HEK293T, HeLa, U2OS, A549, and SW620 cell lines were purchased from the ATCC  
581 and tested for mycoplasma contamination every 3 months. Cells lined are further validated by STR  
582 profiling as part of a rolling program. Statistical analyses generally involved calculation of mean and  
583 standard deviation or standard error of data obtained from a minimum of three biologically  
584 independent samples. Assays with recombinant proteins were carried out (at least) in technical  
585 triplicate. Sample sizes were designed based on prior assay experience, similar work on related  
586 projects, and pilot data.

587

### 588 **Expression vectors and site-directed mutagenesis**

589 *JMJD7*, *DRG1*, *DRG2*, *DFRP1*, *DFRP2* and *dmJMJD7* cDNA were cloned into the pCDNA3 vector  
590 (ThermoFisher) by PCR to incorporate the indicated *N*-terminal epitope tags. *JMJD7* and variants  
591 with *N*-terminal 3x-FLAG tags were cloned into the RFP site of the doxycycline-inducible pTRIPZ  
592 vector (GE LifeSciences) ('pTIPZ'). The pET28a-*JMJD7* plasmid was prepared by Dr. Wei Ge and  
593 generated by inserting the human *JMJD7* gene (encoding full-length *JMJD7*, residues 1-316, NCBI  
594 gene accession number: 100137047) into the pET28a vector (Novagen) for production in *Escherichia*  
595 *coli* with an *N*-terminal His<sub>6</sub>-tag and a thrombin protease cleavage site  
596 (MGSSHHHHHSSGLVPR\*GSH). The following human *JMJD7* constructs (residues 1-316, 1-295,  
597 27-316, 27-295), which were used to investigate oligomerization of *JMJD7*, were amplified from  
598 pET28a-*JMJD7* using custom primers (Sigma Aldrich) and cloned into the pNIC28-Bsa4 vector using  
599 ligation-independent cloning, resulting in constructs with an *N*-terminal His<sub>6</sub>-tag and tobacco etch  
600 virus (TEV) protease cleavage site (MHHHHHHSSGVDLGTENLYFQ\*SM). Genes encoding for  
601 full-length *DRG1* (residues 1-367, NCBI gene accession number: 4733) and *DRG2* (residues 1-364;  
602 NCBI gene accession number: 1819) were amplified from U2-OS cDNA (kindly provided by Dr  
603 Louise Walport, University of Oxford) and also inserted into the pNIC28-Bsa4 vector. Site-directed  
604 mutagenesis was performed using custom primers (Invitrogen or Sigma Aldrich) and either Phusion  
605 High-Fidelity PCR Master Mix with HF Buffer (NEB) or the Stratagene QuikChange® method with  
606 Q5 High-Fidelity DNA Polymerase (NEB). PCR was carried out according to the manufacturer's

607 recommendations followed by DpnI (Thermo-Fisher) digestion for 60 minutes at 37°C before DNA  
608 purification and bacterial transformation. All constructs were fully DNA sequence verified.

609

### 610 **Immunofluorescence**

611 HeLa cells were seeded onto glass cover slips the day before transfection with pCDNA3 FLAG-  
612 JMJD7 and/or HA-DRG1/2. After 48 hours, cells were washed three times with cold PBS before  
613 fixing and permeabilizing with 100% acetone for 7 minutes at -20°C. Immunofluorescence co-staining  
614 was achieved by incubating samples with primary antibodies at 4°C overnight. Secondary antibodies  
615 (Alexa Fluor 555 anti-mouse and Alexa Fluor 488nm anti-rabbit (ThermoFisher)) were incubated at  
616 1:2,000 for 1 hour at room temperature prior to DAPI (Sigma) staining. Cover slips were mounted  
617 onto slides using anti-fade mounting media (NEB ProLong Gold) and imaged using Zeiss LSM510.

618

### 619 **Protein expression analyses**

620 Cellular proteins were extracted using either JIES (20 mM Tris·HCl pH 7.4, 100 mM NaCl, 5 mM  
621 MgCl<sub>2</sub>, 0.5% (v/v) Igepal CA-630, and Complete protease inhibitors (Roche)) or RIPA buffer. Protein  
622 extracts were quantified and equalized using Pierce 660nm Protein Assay Reagent. Western blotting  
623 antibodies were as described above. Signals were developed using SuperSignal West Pico, Dura, or  
624 Femto chemiluminescent substrates (Thermo Fisher Scientific).

625

### 626 **JMJD7 proteomic screen**

627 Inducible FLAG-JMJD7 stable cell lines (wildtype and H178A variant) were treated with doxycycline  
628 (SIGMA) for 38 hours before the addition of 1 mM dimethyl-*N*-oxalylglycine (DMOG; SIGMA,  
629 D3695) for 16 hours, to trap substrates. Cells were lysed in JIES in the presence of 1 mM *N*-  
630 oxalylglycine (NOG; Cambridge Bioscience, 13944), prior to immunoprecipitation with anti-FLAG  
631 M2 Magnetic Beads (Sigma, M8823), overnight at 4°C with rotation. Samples were then washed six  
632 times in JIES before elution with 100 µg/ml 3x-FLAG peptide (SIGMA, F4799). Eluents were  
633 desalted by methanol:chloroform extraction prior to in-solution trypsin digestion using standard

634 methods<sup>49</sup>. Purified tryptic peptides were analyzed by mass spectrometry (as detailed below) in  
635 technical triplicates to allow for label-free quantification.

636

#### 637 **JMJD7:DRG interaction assays**

638 Doxycycline-inducible FLAG-JMJD7 stable cell lines were treated with doxycycline as above before  
639 the addition, or not, of 1 mM DMOG for 10-16 hours. Cells were lysed in JIES in the presence or  
640 absence of 1 mM NOG prior to immunoprecipitation with anti-FLAG Beads, overnight at 4°C with  
641 rotation. Samples were then washed six times in JIES before elution with 100 µg/ml 3x-FLAG  
642 peptide. The interaction of transfected FLAG-DRG1/2 with endogenous JMJD7 was explored using  
643 an identical approach. Endogenous DRG/DFRP/JMJD7 complexes were analyzed by  
644 immunoprecipitation from large-scale DMOG-treated HEK293T cell extracts using DFRP antibodies  
645 bound to protein A agarose (Millipore) and eluted with 2x Laemmli buffer.

646

#### 647 **DRG purification for MS analyses**

648 For exogenous DRG analyses, HEK293T cells were transfected with the pCDNA3 HA-DRG1/V5-  
649 DFRP1 or pCDNA3 HA-DRG2/V5-DFRP2 vectors in the presence or absence of pCDNA3 FLAG-  
650 JMJD7. Cells were incubated under standard culture conditions for 48 hours before lysis in JIES  
651 buffer and immunoaffinity purification of DRG/DFRP complexes using anti-HA agarose beads  
652 (SIGMA, A2095) at 4°C for 16 hours with rotation. Beads were washed five times with JIES before  
653 elution with anti-HA peptide (SIGMA, I2149), protease digest, and mass spectrometry analysis. For  
654 endogenous DRG analyses, large-scale cell cultures were lysed in JIES buffer before immunoaffinity  
655 purification using the antibodies described above. Beads were washed with JIES buffer and eluted  
656 with 2X Laemmli buffer and separated by SDS-PAGE. DRG1 and DRG2 protein bands were excised  
657 from Coomassie-stained gels prior to protease digest and mass spectrometry analysis.

658

#### 659 **RNA interaction assays**

660 HEK293T cells were transfected with pcDNA3 FLAG-DRG1, -DRG1-K22A, -DRG2 or DRG2-  
661 K21A. Alternatively, stable HEK293T cell lines expressing conditional control and JMJD7 shRNA

662 were treated with 1 µg/ml doxycycline for 72h prior to transfection with pCDNA3 FLAG-DRG2.  
 663 Forty-eight hours after transfections cells were lysed in JIES buffer, then centrifuged (14,000 rpm, 10  
 664 minutes) to remove cell debris. Protein extracts were used directly in RNA pulldown assays, or were  
 665 subject to anti-FLAG immunoprecipitation and elution (as above) to purify FLAG-DRG proteins for  
 666 use in RNA pulldown assays (in the presence of JIES buffer supplemented with 1mM DTT). Samples  
 667 were incubated with either 4 mg polycytidylic acid-Agarose beads (SIGMA, P9827), 4 mg  
 668 polyuridylic acid-Agarose beads (SIGMA, P8563) or 20 µl control Protein A Agarose beads  
 669 (Millipore, 16-156) at 4°C for 2 hours with rotation. Beads were washed five times with JIES before  
 670 elution with 30 µl 2X Laemmli buffer.

671

672 **Cellular Protein Mass Spectrometry**

673 Protein samples were digested and desalted using standard methods for in-gel<sup>50</sup> and in-solution<sup>49</sup>  
 674 digest. Desalted samples were analyzed by nLC-MS/MS with frontend separation using a Dionex  
 675 Ultimate 3000 UPLC at a flowrate of 250 nl/min. Peptides were separated using a PepMAP C18  
 676 column (75 µm × 500 mm, 2 µm particle size) and a one hour gradient of 2-35% Acetonitrile in 5%  
 677 DMSO/0.1% formic acid. For MS detection, we either used a Q-Exactive, Q-Exactive HF or Orbitrap  
 678 Fusion Lumos (all Thermo) in HCD mode (Q-Exactives) or CID/Ion trap detection mode for MS/MS  
 679 data acquisition with the following parameters:

	Q-Exactive	Q-Exactive HF	Orbitrap Fusion Lumos
Resolution MS1	70000	60000	120000
Resolution MS2/Scan rate	17500	30000	rapid
MS1 scan range	380 to 1800 m/z	375 to 1500 m/z	375 to 1500 m/z
MS2 scan range	200 to 2000 m/z	200 to 2000	auto
pAGC target MS1	3.00E+06	3.00E+06	4.00E+05
pAGC target MS2	1.00E+05	5.00E+04	2.00E+03
Top N/Speed	15	12	3 s
Dynamic Exclusion	27 s	27 s	60 s
max. injection time MS1	100 ms	45 ms	50
max. injection time MS2	128 ms	100 ms	250
Normalized collision energy	28	28	35
Activation	HCD	HCD	CID
MS2 detector	Orbitrap	Orbitrap	Linear Ion Trap

680 Data were searched against the UniProt Reference (UPR) *Homo sapiens* database (retrieved  
681 15.10.2014) with PEAKS Studio 7.5 (Bioinformatics Solutions) with 10 ppm mass error tolerance for  
682 precursor mass and 0.05 Da (Q-Exactives) / 0.5 Da (Orbitrap Fusion Lumos) tolerance for fragment  
683 masses. Carbamidomethylation on cysteine was selected as a ‘fixed’ modification, while oxidation  
684 (M), deamidation (N, Q) and hydroxylation (P, K, D, N, R, Y) were selected as variable modifications  
685 for the database search. Using a target/decoy fusion approach, the peptide false discovery rate was set  
686 to 1%. Peptide abundance was measured as accumulated ion counts after extraction of the  
687 chromatographic elution profile of the precursor mass of interest using Qual Browser, Xcalibur 3.0.63  
688 (Thermo).

689

#### 690 ***In vitro* JMJD7:DRG interaction assay**

691 HA-DRG1, -DRG1-K22A, -DRG2, and -DRG2-K21A proteins were produced *in vitro* using the TNT  
692 Quick-Coupled transcription/translation system (Promega, L1170). IVVT reactions and anti-FLAG  
693 M2 Magnetic Beads (Sigma, m8823) were spiked into HEK293T cell lysates expressing either  
694 pCDNA3 or pCDNA3-FLAG-JMJD7 prior to overnight incubation at 4°C for 16 hours with rotation.  
695 Anti-FLAG beads were washed three times with JIES buffer before eluting with 50 µl 2X Laemmli  
696 buffer.

697

#### 698 **Protein Basic Local Alignment Search Tool (BLAST) DRG1/2 analysis**

699 Protein BLAST<sup>®</sup> (<https://blast.ncbi.nlm.nih.gov/Blast.cgi?PAGE=Proteins>) searches identified  
700 DRG1/2 homologs from indicated organisms using the human protein sequence as the entry query  
701 (NCBI Reference IDs – *H. sapiens*: NP\_004138.1/001379.1; *X. laevis*: 001084013.1/001079983.1; *D.*  
702 *melanogaster*: 536733.1/650822.1; *C. elegans*: 001255126.1/498808.2; *A. thaliana*:  
703 195662.1/173190.1; *S. cerevisiae*: 009364.1/011689.1; *D. discoideum*: 636294.1/641633.1; *T.*  
704 *thermophila*: 001025967.2/001021328.1). Sequences were aligned using Clustal Omega  
705 (<https://www.ebi.ac.uk/Tools/msa/clustalo/>) and shaded using GeneDoc (version 2.7) as shown in Fig.  
706 3A.

707

708 **Recombinant protein production and purification**

709 All recombinant JMJD7 proteins were produced with *N*-terminal His<sub>6</sub>-tags in *E. coli* Rosetta™  
710 (DE3)pLysS cells (Novagen). Cells were grown in 2TY media at 37°C to an OD<sub>600</sub> of 0.6-0.8.  
711 Recombinant protein production was induced with 0.5 mM isopropyl β-D-1-thiogalactopyranoside  
712 (ITPG); cells were then grown overnight at 18°C. Proteins were purified by nickel affinity  
713 chromatography using an AKTA FPLC system (GE Healthcare®). Recombinant protein was eluted  
714 from the column using a stepwise gradient (30 – 250 mM imidazole), and protein-containing fractions  
715 were further purified by size exclusion chromatography using a Superdex 75 10/300 GL column  
716 (Amersham Pharmacia Biosciences). Protein purity was assessed by SDS-PAGE analysis and  
717 subsequently pooled, concentrated (10-25 mg/mL), flash frozen in liquid nitrogen, then stored at -  
718 80°C in 50 mM Hepes, 200 mM NaCl, 2% glycerol, pH 7.5.

719

720 Recombinant DRG1 was produced and purified as reported<sup>51</sup>. The TEV protease was used for His<sub>6</sub>-tag  
721 cleavage (1:20, TEV:DRG1) with overnight treatment at 4 °C. DRG1 was collected as the eluent after  
722 a 5 mL HiTrap nickel column treatment. DRG1 purity was validated by SDS-PAGE and MS analyses.

723

724 **Recombinant DRG1 hydroxylation**

725 Purified, full-length DRG1 was hydroxylated by treatment with His<sub>6</sub>-JMJD7. Assay mixtures  
726 contained 50 μM DRG1, 2 μM JMJD7, 100 μM ammonium iron(II) sulphate hexahydrate (Fe(II)),  
727 500 μM 2-oxoglutarate acid disodium salt (2OG), 1 mM (+)-sodium L-ascorbate (ascorbate) in 50  
728 mM HEPES, 500 mM NaCl, 5% glycerol, pH 7.5. The reaction was carried out for 2 h at 37°C.  
729 Hydroxylated DRG1 was collected as the eluent after a 5 mL HiTrap nickel column treatment.  
730 Hydroxylation was confirmed by MS analysis using a Xevo GS-2-S mass spectrometer (Waters).  
731 >95% hydroxylation, as observed by MS, was achieved under the stated conditions. The concentration  
732 of the hydroxylated samples was determined using a ND-1000 Spectrophotometer (Nanodrop  
733 Technologies).

734

735

736 **Peptide synthesis**

737 The 25-mer DRG1<sub>16-40</sub> (ARTQKNKATAHHLGLLKARLAKLRR-NH<sub>2</sub>, >95%) and DRG2<sub>15-39</sub>  
738 (ARTQKNKATEYHLGLLKAKLAKYRA-NH<sub>2</sub>, >95%) peptides) were commercially synthesized  
739 with C-terminal amides by either Severn Biotech (United Kingdom) or GL BioChem (China).

740

741 The DRG1<sub>21-40</sub> peptide (NKATAHHLGLLKARLAKLRR-NH<sub>2</sub>) was synthesized in house by solid  
742 phase synthesis using a Liberty Blue automated microwave peptide synthesizer (CEM Corporation,  
743 USA) for amino acid analysis as described<sup>32</sup>. All other peptides used for screening were synthesized  
744 using a Multi pep RSi solid phase peptide synthesizer (Intavis AG Bioanalytical Instruments,  
745 Germany) on a plate module (1-5 mg scale) using Tentagel S-RAM resin as described<sup>32</sup>. All peptides  
746 were synthesized as C-terminal amides. The DRG1<sub>21-40</sub> peptide used for amino acid analysis was  
747 purified by reverse-phase high-performance liquid chromatography using a Vydac C18 column  
748 (Solvent A = 0.1% trifluoroacetic acid in water; Solvent B = 0.1% trifluoroacetic acid in acetonitrile)  
749 to >90% purity as determined by LC-MS. Peptides used for screening assays were not purified.

750

751 **JMJD7 activity assays**

752 *JMJD7 NMR activity assays*

753 NMR assays were carried out as described<sup>32</sup>. 160  $\mu$ L reactions were prepared in a 1.5 mL Eppendorf  
754 tube with 16  $\mu$ L D<sub>2</sub>O (Sigma-Aldrich),  $\pm$ 100  $\mu$ M Fe(II), 200  $\mu$ M 2OG,  $\pm$ 500  $\mu$ M ascorbate,  $\pm$ 1 mM  
755 NOG,  $\pm$ 10  $\mu$ M JMJD7, and  $\pm$ 10  $\mu$ M JMJD7-H178A in 20 mM Tris D-11 (Cambridge Isotope  
756 Laboratories), pH 7.5. Reactions were initiated by addition of JMJD7 or JMJD7-H178A and  
757 immediately transferred to a 3 mm Shigemi NMR tube, which was centrifuged for a few seconds in a  
758 hand centrifuge. Proton NMR spectra were acquired, and the reaction was monitored in real-time on a  
759 Bruker Avance III 700 MHz spectrometer equipped with a 5 mm inverse TCI cryoprobe at 298K and  
760 controlled by TopSpin 3.5. The AV700 was controlled by TopSpin software, and spectrometer  
761 conditions were optimized using a control sample with all reaction components except JMJD7 prior to  
762 data acquisition. The first proton spectrum was acquired with water suppression (16 scans), 325 s after  
763 mixing, following brief optimization (start of data acquisition was 225 s). Spectra were automatically

764 acquired every 105 s for 1900 s. TopSpin 3.2 software was used to process and integrate the peaks  
765 corresponding to 2OG and succinate for analysis using Microsoft Excel 2003.

766

#### 767 *MALDI-MS hydroxylation assays*

768 JMJD7 assay mixtures (final volume 20  $\mu$ L in 50 mM HEPES, pH 7.5) containing 50  $\mu$ M peptide and  
769 10  $\mu$ M His<sub>6</sub>-JMJD7 were incubated for 60 minutes at 37°C with 100  $\mu$ M Fe(II), 200  $\mu$ M 2OG, and  
770 500 ascorbate. Reactions were quenched by immediately spotting 1  $\mu$ L of assay sample and 1  $\mu$ L of  
771  $\alpha$ -cyano-4-hydroxycinnamic acid (CHCA) matrix solution (saturated CHCA in 50% acetonitrile, 50%  
772 water, 0.1% trifluoroacetic acid) onto a Waters 96-spot MALDI plate. The samples were analyzed  
773 using MALDI- MS and a Waters Micromass<sup>TM</sup> MALDI micro MX<sup>TM</sup> instrument in the positive ion  
774 reflectron mode. MALDI-MS spectra were analyzed using MassLynx 4.1 (Waters) by baseline  
775 subtraction (polynomial order, 15; below curve %, 10; tolerance, 0.01) and smoothing (number of  
776 smooths, 2; smooth window channels, 10; Savitzky-Golay).

777

#### 778 *Co-factor/substrate dependence assays*

779 Co-factor/substrate dependence assays (**Fig. 3d**) were performed as described (above) with the  
780 following modifications: 50  $\mu$ M DRG1<sub>16-40</sub>,  $\pm$ 1  $\mu$ M JMJD7 or JMJD7-H178A,  $\pm$ 100  $\mu$ M Fe(II),  $\pm$ 500  
781  $\mu$ M 2OG,  $\pm$  1mM ascorbate,  $\pm$  1mM NOG, and quenching after 5 minutes of incubation at 37°C with  
782 formic acid (2% final concentration) prior to spotting on the MALDI plate.

783

#### 784 *<sup>18</sup>O<sub>2</sub> incorporation assays*

785 Hydroxylation of DRG1<sub>16-40</sub> by JMJD7 was performed under atmospheres of argon, <sup>16</sup>O<sub>2</sub>, or <sup>18</sup>O<sub>2</sub> (CK  
786 Isotopes, 98%) as described<sup>12</sup>. Assays were performed under the following conditions: 50  $\mu$ M  
787 DRG1<sub>16-40</sub>,  $\pm$ 2.5  $\mu$ M JMJD7, 100  $\mu$ M Fe(II), 500  $\mu$ M 2OG, and 1 mM ascorbate in 50 mM HEPES,  
788 pH 7.5. A solution of peptide and buffer (94  $\mu$ L) in a septum-sealed glass vial was purged with N<sub>2</sub> for  
789 30 minutes on ice using a mass flow controller (Brooks Instruments) and an escape needle. 1 $\mu$ L of  
790 2OG, Fe(II), ascorbate, and JMJD7 were then sequentially added on ice using gastight Hamiltonian

791 syringes. A balloon attached to a syringe was purged 3x with Argon then filled with the gas of choice  
792 (argon,  $^{16}\text{O}_2$ , and  $^{18}\text{O}_2$ ). The reaction was initiated by slowly bubbling the gas into the solution at room  
793 temperature using an escape needle until the balloon was deflated (~10 minutes). The escape needle  
794 was removed, followed by the balloon; the solution was then incubated at 37°C for an additional 20  
795 minutes and quenched with 100  $\mu\text{L}$  of 4% formic acid. Products were analyzed by MALDI-MS as  
796 above.

797

### 798 **Non-denaturing MS**

799 Stoichiometry measurements were performed using a hybrid quadrupole-Orbitrap (Thermo  
800 QExactive) and a quadrupole-time-of-flight (Waters Synapt G2Si) instrument for detection of high  
801 mass ions<sup>52,53</sup>. Samples (10  $\mu\text{M}$ ) were buffer exchanged into 200 mM ammonium acetate using Bio-  
802 spin 6 (Bio-Rad) centrifuge columns immediately prior to analysis. Ions were generated by static  
803 nanoelectrospray using gold-coated capillaries prepared in-house. Data were obtained with a wide  
804 acquisition window (2,000-10,000  $m/z$ ); desolvation was achieved with moderate HCD voltage  
805 (QExactive; 10-50 V) or CID (Synapt; 4 V) applied. Instrument settings were: (QExactive): capillary  
806 voltage = 1.1 kV; source temperature = 50°C; max injection time = 50; S-lens RF = 100; C-trap  
807 entrance lens = 5.8. Spectra were obtained with 10 microscans, averaged over 100 scans. Instrument  
808 settings were as follows (Synapt): capillary voltage = 1.4 kV; source temperature = 50°C; sample  
809 cone = 10 V; trap DC bias = 10 V. Data were processed using XCalibur 2.1 (Thermo Scientific) and  
810 MassLynx V4.1 (Waters) software and masses were assigned using in-house software (Mass/Charge  
811 State Error Determination v 0.3; <http://benesch.chem.ox.ac.uk/resources.html>).

812

### 813 **SEC-MALS and CD studies**

814 Analysis of JMJD7 was performed using an Agilent 1260 HPLC with a Superdex 200 Increase  
815 3.2/300 SEC column (GE Healthcare) coupled to a DAWN HELEOS II scattering detector (Wyatt  
816 Technologies) and Optilab T-rEX (Wyatt Technologies) differential refractive index detector. The  
817 MALS detector was equilibrated overnight in running buffer to ensure minimal background light

818 scattering. ~30  $\mu\text{g}$  of protein was loaded on-column (column compartment was set to 20°C) at a flow  
819 rate of 75  $\mu\text{L}/\text{min}$  in 50 mM HEPES, 200 mM NaCl, 2% glycerol, pH 7.5. Data acquisition and  
820 analysis were performed with Astra 6.1 software (Wyatt Technologies).

821

822 CD spectra were acquired using a Chirascan CD spectrometer (Applied Photophysics model)  
823 equipped with a Peltier temperature-control cell holder. Experiments were performed at 20°C in a 0.1  
824 cm pathlength cuvette using 0.2 mg/mL of protein in 10 mM sodium phosphate buffer, pH 8.0. Data  
825 were recorded in triplicate from 260 to 185 nm in 0.5 nm steps with a 1 nm bandwidth. Spectral data  
826 were baseline corrected, averaged, and smoothed using the Savitzky-Golay filter (smooth = 8).

827

### 828 **Peptide NMR analyses**

829 DRG1<sub>16-40</sub> and DRG2<sub>15-39</sub> peptides (~1.4 mg) were incubated with 2  $\mu\text{M}$  JMJD7, 100  $\mu\text{M}$  Fe(II), 500  
830  $\mu\text{M}$  2OG, 1 mM ascorbate in 50 mM HEPES, pH 7.5 (10 mL reaction volume) for 2 hours at 37°C;  
831 reactions were quenched by adding neat formic acid dropwise until pH ~2. Peptides were purified  
832 using two Sep Pak C18 columns in tandem according to the Kessler Laboratory Proteomics Protocol  
833 (University of Oxford, [http://www.ccmp.ox.ac.uk/\\_asset/file/sep-pak-c18.pdf](http://www.ccmp.ox.ac.uk/_asset/file/sep-pak-c18.pdf); all volumes doubled),  
834 eluting with 4 mL of 40% acetonitrile, 0.1% formic acid solution in double distilled water. Samples  
835 were then dried by vacuum centrifugation and resuspended in H<sub>2</sub>O/D<sub>2</sub>O (9:1) for 2D NMR analyses  
836 (HSQC, HMBC, COSY, TOCSY). Spectra were recorded using a Bruker AVIII 700 MHz NMR  
837 spectrometer equipped with a 5-mm inverse cryoprobe using 3mm MATCH NMR tubes (Cortecnet).  
838 Data were processed using a TopSpin 3.2 software (Bruker).

839

### 840 **Amino acid analyses**

#### 841 *Sample Preparation*

842 Peptides (50  $\mu\text{M}$ ; DRG1<sub>21-40</sub>, DRG1<sub>16-40</sub>, and DRG2<sub>15-39</sub>) were incubated with 100  $\mu\text{M}$  Fe(II), 200  $\mu\text{M}$   
843 2OG, and 500  $\mu\text{M}$  ascorbate in the presence or absence of 10  $\mu\text{M}$  recombinant His<sub>6</sub>-JMJD7 for 1 hour  
844 at 37°C in 50 mM HEPES, pH 7.5 (final volume 500  $\mu\text{L}$ ). The reaction was quenched with 2 drops of

845 neat formic acid; hydroxylation (~40-80%) of the peptide was confirmed by MALDI-MS.  
846 Recombinant JMJD7 was removed using a Sep Pak C18 column according to the Kessler Lab  
847 Proteomics Protocol (University of Oxford, [http://www.ccmp.ox.ac.uk/\\_asset/file/sep-pak-c18.pdf](http://www.ccmp.ox.ac.uk/_asset/file/sep-pak-c18.pdf)),  
848 eluting with a 15% acetonitrile, 0.1% formic acid solution in double distilled water. Samples were  
849 then dried by vacuum centrifugation and subsequently re-suspended in 60  $\mu\text{L}$  of 20 mM HEPES, pH  
850 7.5. Enzymatic hydrolysis was carried out at 37°C with a non-specific protease from *Streptomyces*  
851 *griseus* (9  $\mu\text{L}$ , 1 mg mL<sup>-1</sup>, Sigma-Aldrich) overnight.

852

### 853 *LC-MS analyses*

854 Hydrolyzed samples were dried by vacuum centrifugation followed by resuspension in borate buffer  
855 and derivatization with 6-aminoquinolyl-*N*-hydroxysuccinimidyl carbamate (AQC) according to the  
856 AccQ-Tag Ultra Derivatization Protocol (Waters). LC-MS analyses were performed as described<sup>24</sup>,  
857 using a Waters Acquity ultra performance liquid chromatography system coupled to a Xevo G2-S  
858 QToF mass spectrometer equipped with an electrospray ionisation source. Gradient conditions for  
859 separation were carried out as described in either the AccQ-Tag Ultra Derivatization Protocol  
860 (Waters; 10 minute gradient) or in Feng et al., 2014<sup>14</sup> (30 minute gradient).

861

862 Conditions for ESI-MS detection: mode, positive-ion; analyzer, resolution mode; desolvation  
863 temperature, 600°C; source temperature, 100°C, capillary voltage, 3000 V; sample cone voltage, 20 V;  
864 cone gas flow, 30 L/min; and desolvation gas flow 1000 L/min. MS data were acquired and extracted  
865 ion chromatograms were produced for m/z values of either 503.2, corresponding to the theoretical  
866 masses of AQC-derivatized hydroxylysine (503.2037). Extracted ion chromatograms were smoothed  
867 (number of smooths, 2; smooth window channels, 3; Savitzky-Golay) and total ion current  
868 chromatograms were further baseline subtracted (polynomial order, 1; below curve %, 40; tolerance,  
869 0.01).

870

871 C3, C4, and C5 hydroxylysine standards were synthesized or commercially obtained as described<sup>14</sup>.  
872 The synthesis of the (2*S*,3*R*)/(2*R*,2*S*)-3-hydroxylysine standard has been reported elsewhere<sup>27</sup>.

873 **Differential scanning calorimetry**

874 Differential scanning calorimetry experiments were performed on a Malvern (Malvern, UK) VP  
875 Capillary DSC instrument at the Department of Biochemistry, University of Oxford. Samples and  
876 buffer blanks were measured using a thermal ramp of 200 °C/hr between 10°C and 110°C at a  
877 pressure of 55 psi. Samples contained 80 µM full length DRG1/hydroxylated DRG1 in the presence  
878 or absence of 1 mM GDP (Sigma) in 50 mM HEPES, 500 mM NaCl, 5 % glycerol, pH 7.5. The  
879 buffer blanks consisted of 50 mM HEPES, 500 mM NaCl, 5 % glycerol, pH 7.5 ( $\pm$  1 mM GDP).

880

881 **DRG GTPase activity assays**

882 *Phosphate release assay*

883 GTP hydrolysis was measured using a colorimetric assay for determination of phosphate release<sup>51</sup>.  
884 Recombinant, full length DRG1 and hydroxylated DRG1 (10 µM) were incubated with increasing  
885 concentrations (0–4 mM) of GTP in 100 mM Tris/ HCl, pH 8, 300 mM KCl, 20 mM MgCl<sub>2</sub>, 10%  
886 glycerol at 37 °C for 60 min. Reactions were stopped by adding 50 µL of fresh malachite green  
887 reagent. This reagent contained 2 volumes of 0.0812% malachite green, 2 volumes of bidistilled  
888 water, 1 volume of ammonium molybdate (5.72% in 6 M HCl) and 1 volume of 2.32% polyvinyl  
889 alcohol (Phosphate Assay Kit, colorimetric, Abcam). The samples were read within the next 10 min in  
890 a PheraStar plate reader at 650 nm using half-area, medium binding, clear bottom plates (Fischer  
891 Scientific). End-point assays contained the purified proteins (10 µM) that were incubated with 1 mM  
892 of GTP in 100 mM Tris/ HCl, pH 8, 300 mM KCl, 20 mM MgCl<sub>2</sub>, 10% glycerol at 42°C for 60 min.  
893 The samples were quenched and read as previously stated.

894

895 *GTPase activity monitoring by NMR*

896 Purified proteins (40 µM) were incubated with 4 mM of GTP in 50 mM Tris-D<sub>11</sub>, pH 7.5, 300 mM  
897 KCl, 20 mM MgCl<sub>2</sub>, at 37 °C for 60 min. Controls contained 4 mM GTP or GDP under the same  
898 conditions. <sup>1</sup>H excitation sculpting suppression NMR spectra were recorded using a Bruker AVIII 600  
899 MHz NMR spectrometer equipped with a BB-F/<sup>1</sup>H Prodigy N<sub>2</sub> cryoprobe using 5 mm diameter NMR  
900 tubes (Norell). Spectra were typically obtained using 252 scans, a relaxation delay of 1 s, and a

901 prescan delay of 10  $\mu$ s. A 2 ms sinc pulse was used for water suppression. Data were processed with a  
902 line broadening of 0.3 Hz using TopSpin 3.2 software (Bruker).

903

#### 904 *GTPase activity assay of DRG proteins purified from human cells*

905 FLAG-DRG1/2 proteins and mutants were expressed in HEK293T cells under a variety of conditions,  
906 including: co-expression of HA-JMJD7, knockdown of JMJD7 by shRNA (as detailed above), or  
907 DMOG treatment (1 mM for 16 hours). Cells were lysed in JIES prior to anti-FLAG  
908 immunoprecipitation. Beads were then washed six times in JIES before elution with 100  $\mu$ g/ml 3x-  
909 FLAG peptide in 100 mM Tris-HCl pH 8, 200 mM KCl, 20 mM MgCl<sub>2</sub>, 10% (v/v) glycerol. The  
910 purity and abundance of DRG1/2 proteins were determined by SDS-PAGE and coomassie staining.  
911 GTPase activity of purified proteins was measured using the GTPase-Glo Kit (Promega, V7681),  
912 according to the manufacturer's guidelines, but with the following modifications. Firstly, the GTPase  
913 assay buffer was supplemented with 200 mM KCl to support DRG GTPase activity<sup>51</sup>. Secondly,  
914 assays were performed at 37°C for either 2h (DRG2) or 8h (DRG1).

915

#### 916 **Crystallization conditions**

917 Crystals of His<sub>6</sub>-JMJD7.Mn(II).2OG and His<sub>6</sub>-JMJD7-R260C.Mn(II).2OG were obtained in sitting  
918 drops at 25°C. For wildtype JMJD7, drops were formed in a 1:1 ratio of a 25 mg/mL His<sub>6</sub>-JMJD7, 2  
919 mM MnCl<sub>2</sub>, 4 mM 2OG solution with a 1.5 M sodium nitrate, 0.1 M sodium acetate, pH 4.6 solution.  
920 For the R260C variant, drops were formed in a 1:1 ratio of a 26 mg/mL His<sub>6</sub>-JMJD7-R260C, 2 mM  
921 MnCl<sub>2</sub>, 4 mM 2OG solution with a 1.5 M sodium nitrate, 0.1 M sodium acetate, pH 4.6 solution  
922 containing additives (0.25%  $\beta$ -Nicotinamide adenine dinucleotide phosphate tetrasodium salt, 0.25%  
923 Adenosine 5'-triphosphate disodium salt hydrate, 0.25% N-Acetyl-D-galactosamine, 0.25%  
924 Gentamicin sulfate salt hydrate, 0.02 M HEPES sodium pH 6.8). Crystals were cryoprotected with  
925 25% glycerol before flash freezing in liquid nitrogen.

926

927

928

929 **Data collection, structure solution, and refinement**

930 Data were collected using single crystals at 100 K at the Diamond Light Source (DLS) beam lines I04  
931 (PDB: 5NFN,  $\lambda=0.9795 \text{ \AA}$ ) and I03 (PDB: 5NFO,  $\lambda=0.9795 \text{ \AA}$ ) and processed using HKL2000<sup>54</sup>.

932 His<sub>6</sub>-JMJD7.Mn(II).2OG data were strongly anisotropic (the spread in values of the three principal  
933 components of scale factors is  $62.37 \text{ \AA}^2$ ), with resolution limits of  $3.5 \text{ \AA}$ ,  $3.5 \text{ \AA}$ , and  $3.0 \text{ \AA}$  along the  
934 reciprocal axes  $a^*$ ,  $b^*$  and  $c^*$  (at an  $F/\sigma$  cutoff of 3). The data were ellipsoidally truncated and  
935 anisotropically scaled using the 'STARANISO anisotropy & Bayesian estimation server'  
936 (<http://staraniso.globalphasing.org/cgi-bin/staraniso.cgi>) with intensities renormalized for structure  
937 solution and initial rounds of refinements. An ensemble of models was generated by the  
938 ENSEMBLER built in PHENIX<sup>55</sup> using crystal structures of the related JmjC-enzymes, FIH (PDB ID:  
939 1H2K), TYW5 (PDB ID: 3AL5), JMJD5 (PDB ID: 4GJZ), and JMJD6 (PDB ID: 3K2O) as templates.  
940 To ensure maximum degree of accuracy, only JMJD7 residues that are highly conserved in these four  
941 JmjC-hydroxylases were included in the homology models. The wildtype JMJD7 structure was then  
942 solved by molecular replacement using PHASER<sup>56</sup>. An initial model was generated by PHENIX  
943 AUTOBUILD<sup>55</sup>, which included 82% of JMJD7 residues making up the four molecules in the  
944 asymmetric unit. Iterative cycles of model building and refinement using Buster<sup>57</sup> were performed  
945 until converging  $R_{\text{factor}}/R_{\text{free}}$  no longer decreased. Final rounds of intensity-based refinements were  
946 performed using CNS<sup>58</sup> and PHENIX<sup>55</sup>. JMJD7-R260C structure was solved by molecular  
947 replacement using PHASER<sup>56</sup> with 2 molecules per asymmetric unit using the JMJD7-wt structure as  
948 the initial model and refined by CNS<sup>58</sup>/ PHENIX<sup>55</sup> until  $R_{\text{factor}}/R_{\text{free}}$  converged with iterative cycles  
949 model building using COOT<sup>59</sup>. MOLPROBITY<sup>60</sup> was used to monitor the geometric quality of the  
950 models between refinement cycles. Water molecules were added to peaks ( $> 1.5 \sigma$   $2F_oF_c$ ) in electron  
951 density maps that were within H-bond distance to protein with reasonable geometry to form H-bonds.

952

953

954

955

956 **Data availability**

957 Atomic coordinates and structure factors for crystal structures have been deposited in the Protein Data

958 Bank under the accession codes: 5NFN and 5NFO. Mass spectrometry data have been deposited in

959 PRIDE under the accession code XXXX (to follow).

960 **References**

- 961 48. Katz, M. J. *et al.* Sudestada1, a Drosophila ribosomal prolyl-hydroxylase required for mRNA  
962 translation, cell homeostasis, and organ growth. *Proc. Natl. Acad. Sci.* **111**, 4025–4030 (2014).
- 963 49. Fischer, R. *et al.* Discovery of candidate serum proteomic and metabolomic biomarkers in  
964 ankylosing spondylitis. *Mol. Cell. Proteomics* **11**, M111.013904 (2012).
- 965 50. Xu, D. *et al.* Novel MMP-9 substrates in cancer cells revealed by a label-free quantitative  
966 proteomics approach. *Mol. Cell. Proteomics* **7**, 2215–2228 (2008).
- 967 51. Pérez-Arellano, I., Spínola-Amilibia, M. & Bravo, J. Human Drg1 is a potassium-dependent  
968 GTPase enhanced by Lerepo4. *FEBS J.* **280**, 3647–57 (2013).
- 969 52. Gault, J. *et al.* High-resolution mass spectrometry of small molecules bound to membrane  
970 proteins. *Nat. Methods* **13**, 333–336 (2016).
- 971 53. Parsons, T. B. *et al.* Optimal synthetic glycosylation of a therapeutic antibody. *Angew. Chemie*  
972 *Int. Ed.* **55**, 2361–2367 (2016).
- 973 54. Otwinowski, Z. & Minor, W. Processing of X-ray diffraction data collected in oscillation  
974 mode. *Methods Enzymol.* **276**, 307–326 (1997).
- 975 55. Adams, P. D. *et al.* PHENIX : a comprehensive Python-based system for macromolecular  
976 structure solution. *Acta Crystallogr. D Biol. Crystallogr.* **66**, 213–221 (2010).
- 977 56. McCoy, A. J. *et al.* Phaser crystallographic software. *J. Appl. Crystallogr.* **40**, 658–674 (2007).
- 978 57. Smart, O. S. *et al.* Exploiting structure similarity in refinement: automated NCS and target-  
979 structure restraints in BUSTER. *Acta Crystallogr. D Biol. Crystallogr.* **68**, 368–380 (2012).
- 980 58. Brünger, A. T. *et al.* Crystallography & NMR system: A new software suite for  
981 macromolecular structure determination. *Acta Crystallogr. D Biol. Crystallogr.* **54**, 905–921  
982 (1998).
- 983 59. Emsley, P. & Cowtan, K. Coot: Model-building tools for molecular graphics. *Acta Crystallogr.*  
984 *D Biol. Crystallogr.* **60**, 2126–2132 (2004).
- 985 60. Chen, V. B. *et al.* MolProbity: all-atom structure validation for macromolecular  
986 crystallography. *Acta Crystallogr. D Biol. Crystallogr.* **66**, 12–21 (2010).
- 987